Nanomechanics of Organic Layers and Biomenbranes

Gerard Oncins Marco

Universitat de Barcelona

Facultat de Química

Departament de Química Física

NANOMECHANICS OF ORGANIC LAYERS AND BIOMEMBRANES

Gerard Oncins Marco

TESI DOCTORAL

Universitat de Barcelona

Departament de Química Física

Programa de doctorat: Tecnologia de Materials

Bienni: 2003-2004

NANOMECHANICS OF ORGANIC LAYERS AND BIOMEMBRANES

Memòria que presenta Gerard Oncins Marco per optar al títol de Doctor per la Universitat de Barcelona

Directors:

FAUSTO SANZ CARRASCO

Catedràtic del Departament de Química Física de la Universitat de Barcelona

JOAN TORRENT BURGUÉS

Catedràtic del Departament d'Enginyeria Química de l'Escola Universitària d'Enginyeria Tècnica Industrial de Terrassa

Barcelona, juliol de 2007

Al meu germà, en Carles

Contents

Chapter 1

1.Preface

1.1 MOTIVATION

From the dawn of history, the mechanical properties of materials have been a matter of life or death for human race; we needed shelter, so we chose the most durable, light and weather-proof wood available to build the structure of our primitive huts. Then we learned that the branches that we used to cover the roofs could be replaced by animal skin which, only the Gods knew why, provided an impermeable layer that maintained us dry. The awakening of human conscience developed side by side with the individual capacity to observe and manipulate the surrounding environment and it was this knowledge which impulsed these primitive hominids to learn that certain rocks could be prepared and handcrafted to meet specific requirements. Highly polished edges for cutting animal skin, blunt and sturdy flat surfaces to shatter the bones and extract the rich marrow, sharp spikes to crown their spears and so on. Of course, all these stone age tools can seem rough and primitive for our XXI century technological lifestyle but there is a veiled message that brings together human beings thousands of years apart: they, like us, understood that Nature is an endless source of materials which are patiently waiting for our mind to be bright enough to provide them with a clever application.

The giant leap that took us from the quest for fire to the Industrial Revolution was just a matter of time, provided that the seed of curiosity was planted in human mind. And it was in the XV and XVI century when geniuses like

Copernicus and Leonardo da Vinci transformed the magical conception of the world that characterized the Middle Ages into science that could be constrained to certain laws and principles. For all this, the Renaissance paved the way to understand the world from a different point of view. Interestingly, tribology (from the Greek *tribo*, which means "friction, rub, grind") was born during this period and grew accordingly to the new scientific developments to become the extremely important Physics and Materials Science field that is today. It is easy to imagine processes where friction plays an important role in our macroscopic environment: the tires of a car, the soles of our shoes and the surface of a grinding paper are only some examples where materials are chosen because of their specific frictional properties. Now let us move to the microscopic world; it is difficult to attain this abstraction because our human minds are so adapted to the macroscopic dimensions that our eyes and hands are designed to sense. With the awakening of the microelectronics industry, devices become smaller and the laws of Physics accepted by the scientific community have to be constantly revised. In this new scenario where the micron becomes the common length unit, the frictional and mechanical properties of materials need to be redefined and new methods to explore them must be developed.

Another field that has been given renewed attention with the development of nanometric techniques is Biology. In the last decade, the study of biological structures has moved to the single-molecule scale and the development of hybrid devices that comprise bio and mechanical parts is just around the corner. With this promising future in mind, it is time for scientists to explore and understand the physical properties of these materials from an electrical, mechanical and, of course, tribological point of view so as to make the nanobio revolution a reality.

This thesis project was born 5 years ago, in the Physical Chemistry Department of the University of Barcelona. During my Chemistry degree, I coursed Materials Science matters, as I was more interested in mechanics of materials than in wet chemistry. In fact, I worked as an undergrad preparing metallographic probes and studying dislocations in aluminum alloys. I was quite keen on this field

but then I heard about Nanotechnology and decided to give it a try. It was amazing: the quantum corral, the monoatomic steps, the tunneling effect... I guess that the thing that impressed me the most was the dimensional scale of the whole thing:

Nanometers, molecules, atoms.

Still today I feel awe when we talk about all these things during group meetings and draw fatty acids in the blackboard and brainstorm about how they bend or deform under an external pressure. A foot in the blackboard, 2 nanometers in the real world. And the most frightening question: can our macroscopic sense of reality understand what is going on in the atomic realms?

I worked for a year preparing alkanesilane self-assembled monolayers on mica and acquiring the hard way the necessary skills that an atomic force microscopist must achieve: patience and more patience. Alkanesilanes provided a simple and reproducible sample so as to understand the philosophy lying behind Atomic Force Microscopy and provided a suitable substrate to perform Force Spectroscopy measurements. Right then force curves where widely used in our lab, especially on ionic crystals, so we decided to apply this technique to organic materials. The possibilities seemed really promising: we could indent the monolayers and extract mechanical information from there and I could unify my two scientific passions: mechanics and nanotechnology. What else could I ask for?

Of course, we did not obtain any relevant result from this first project but I understood something really important: good science needs time.

Then something happened that changed the direction of my project, which was somewhat uncertain for me. Fausto, my advisor, lent me the PhD thesis manuscript of a scientist that he had met in Berkeley. His name was Robert Carpick and his work talked about friction in ultra-high vacuum conditions and the possibility of performing nanotribological measurements using an Atomic Force Microscope. It was an amazing and compelling book, full of scientific achievements so I decided that it would be really interesting to apply the techniques

that he proposed to the monolayers I was studying. From here onwards things changed fast: I performed a stage in Wisconsin in Rob Carpick's group, then I implemented the experimental setup in our lab in Barcelona... And the rest of the story is embedded in the pages of this work, which I thank you so much for reading.

1.2 OBJECTIVES

The main objective of this work was to quantitatively measure the nanotribological properties or organic layers and rationalize them from a physicochemical point of view. To accomplish that, a wide array of samples was selected, ranging from technological coatings as alkanethiols to biological coatings as phospholipid bilayers, which can be used to functionalize miniaturized electromechanical systems. Although the studied molecules are different in nature and functionality, the intermolecular forces that determine the layers structure are the same: van der Waals, electrostatic and water-related interactions. We are interested in quantifying these interactions as a function of the intermolecular distances, the nature of the medium the molecules are immersed in (liquid or air) and also assess external factors that have specific effects on the samples. These external factors were overall tested in biological membranes (phospholipid bilayers), where temperature and the presence of ions play a decisive role in their structure.

In order to achieve our objectives, two experimental techniques were mainly used. The first one is the Lateral Force Microscopy, which was implemented in our lab during the execution of this project. As the nature of the measurements we wanted to perform was quantitative, it was also necessary to implement the methods to calibrate Atomic Force Microscopy probes both vertically and laterally. Besides, as we wanted to test the biological samples in liquid environment, a new methodology to perform Lateral Force Microscopy measurements in liquid had to be implemented. The second main technique is Force Spectroscopy, which was used to complement the nanomechanical information obtained from the friction

measurements and that gave us a more detailed picture of the mechanical response of layers. Our technical goal was to obtain fast, reproducible and consistent Force Spectroscopy results, fact that implied the development of a dedicated software routine and the systematic control of the probes shape.

Chapter 2

2.Surface Mechanics overview

2.1 CLASSICAL SURFACE MECHANICS

In the long road that will take us from the coarse friction exerted by a grinding paper on a piece of wood to the delicate interactions arisen between an Atomic Force Microscopy tip and a phospholipid bilayer, it is mandatory to pay homage to the fathers of classical mechanics, the ones that just with imagination and talent set the foundations of the modern physics. Let's start our journey[1].

Leonardo da Vinci (1452-1519) was the first scientist that studied friction phenomena in a quantitative way[2]. Armed with wood cylinders, inclined planes and ropes, he observed that:

- *Friction force (F_f) does not depend on the area of contact (A).*
- *F_f is proportional to the mass of the slider (M_s).*

Because of the nature of his experiments, which are depicted in Fig. 1, he was not able to discern between static and kinetic friction but he was able to establish the first definition of friction coefficient (μ) as the direct relationship between F_f and M_s

$$\mu = \frac{F_f}{M_s} \tag{1}$$

Leonardo found a μ value of 0.25 for all tested materials (the so-called Bilfinger value). Although posterior measurements demonstrated that μ varies depending on the sliding surfaces, the Bilfinger value was considered as a universal constant for quite a long time.

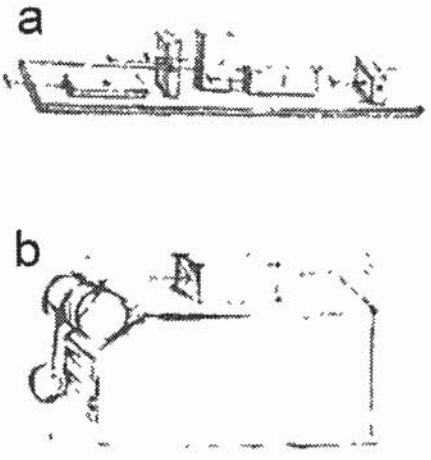

Fig. 1. a) Leonardo discovered that the force needed to move a book does not depend on the side that is in contact with the table, so he concluded that F_f was independent of A. b) Experimental setup to apply a constant force to move a body.

Guillaume Amontons (1663-1705) rediscovered the Leonardo's work about friction, giving a more complete description and reaching the next conclusions[3] using the experimental setup drawn in Fig. 2:

- *F_f opposes to the movement of a mass sliding on a surface.*
- *F_f is proportional to the vertical force (F_v) exerted by the surface on the slider.*
- *F_f does not depend on the apparent area of contact between the sliding surfaces.*

As we can see, the main contribution of Amontons was to introduce old ideas in the scientific community of his time, which was not a simple thing to do provided the unyielding attitude of the scientist during the XVII century (although some remnants of this attitude are still out there).

The French physicist Charles Augustine de Coulomb (1736-1806) was the one that set the basis of the friction theory that we are familiar with (or should, as it is the way it is explained at high school)[4]. Briefly, he redefined the μ introduced by Leonardo as it follows:

$$F_f = \mu F_v \tag{2}$$

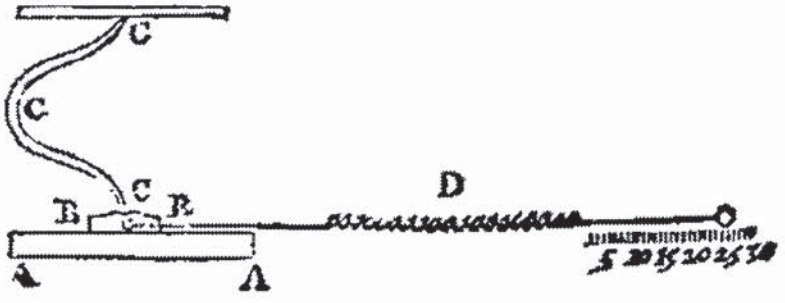

Fig. 2. Amontons' machine designed to perform friction measurements. F_f between the surfaces A and B are measured by the spring D, while F_v is controlled by the spring C, which pushes the slider against the tested surface. As you can see, the design is quite advanced, which implies that Amontons had a clear idea about the meaning of macroscopic friction.

He also said that F_f was independent of velocity once motion starts, ideas that were refined by Leonhard Euler (1707-1783)[5-7], who introduced the concept of kinetic and static friction for the first time; when the two sliding surfaces are in motion relative to each other, μ is called *kinetic friction coefficient* and F_f is the force that tries to counteract the pushing force that creates the sliding movement. In the case of two surfaces that do not move relative to each other, μ is called *static friction coefficient* and is usually higher than the *kinetic* one. Now, according to these new concepts, F_f must be considered as a threshold force. In other words, until F_f is not surpassed by the pushing force, the sliding will not begin. The segregation of friction in two different operation regimes, that is, *kinetic* and *static*, was the first prove scientists gathered to reckon that friction processes were more mysterious than Leonardo expected and this mystery and others that will be slowly unveiled along this thesis paved the way towards the models that are used nowadays. As we can see, F_f defined by Coulomb did not depend on the two sliding

surfaces A. In this direction, John Theophilius Desanguliers (1683-1744) had previously proposed that adhesion (F_A), which is the force needed to separate two bodies in contact, played a key role in the friction phenomena and F_A was a function of A. Consequently, that fact implied that F_f was dependent of A and that Amontons was wrong. Despite being painful, above all for the scientists involved, Science always benefits from conflicting ideas, although it was not until the XX century that the right questions were asked.

In 1954, F. P. Bowden and D. Tabor proposed a solution for the area of contact dilemma[8]; in fact, they established that two bodies do not contact with their whole surface, but only with a finite number of small *asperities*. This new concept redefined the way of studying contacting surfaces and drove tribology towards the micrometric world. As a matter of fact, they theoretically demonstrated that

$$F_f \propto F_v^{\frac{2}{3}} \tag{3}$$

As a result, Amontons' laws were called into question again but not for long as in 1957 J. F. Archard found the way to unify the old and new theories[9]: In their works, Bowden and Tabor had considered that the number of asperities, which are proportional to the real A, were independent on the applied F_v. Archard considered that this assumption was not right and modeled the way the number of asperities increased with F_v. Finally, he concluded that F_f and F_v were proportional.

As Amontons had proposed 200 years ago.

Several and really important scientific conclusions can be extracted from this brief history of tribology. Nevertheless, I will not list them now, as we are just in the beginning of this work. As far as I am concerned, the really shocking piece of knowledge is the moral of this story; the final result is just the surface, as there are lots of different explanations that lead to it. The wisdom of great scientists, the refinement of knowledge is the fuel that drives Science forward. Amontons and Bowden were both right, but what a difference!

2.2 A NEW ERA FOR TRIBOLOGY

The *asperity* concept proved to describe quite well the reality, and the first serious money was made from there. As it was clear that F_f depended on the real A, automobile makers developed smoother tires to increase friction and cold welding professionals polished the surfaces to be welded in order to improve the strength of the union. Eventually, the development of the asperity theory led Bowden and Tabor to think that the friction physical process consisted on the creation and melting of microscopic contacts as the two surfaces slid, ultimately considering that mechanical wear was the origin of friction. Nevertheless, this explanation did not endure the confrontation with reality: there was friction even between surfaces that did not show any appreciable wear.

Jacob N. Israelachvili, a student in Tabor's lab, took his advisor's ideas a step further[10]: in order to experimentally measure the real A value between two surfaces (for the moment it had been impossible to solve this problem and asperities were a kind of abstract concept), he developed the Surface Force Apparatus (SFA)[11-13]. The idea consisted in bringing into close contact two pieces of bended mica in perpendicular directions so as to ensure a micrometric A. Mica is a layered aluminosilicate that can be cleaved, exposing a fresh and atomically flat surface. Then, the apparent A value would equal the real A, as the two contacting surfaces did not show any asperity. Israelachvili confirmed that friction truly depends on the real A value and also confirmed the close relationship between F_f and F_A. The striking fact was that the relationship did not rely on the strength of the adhesive bonds but on the difference between the static and the kinetic adhesion. Unfortunately, he could not unveil the physical processes behind these observations.

2.3 TRIBOLOGY MOVES TO THE ATOMIC SCALE

In the 80's Gary McClelland developed a model which successfully explained the wearless friction phenomena[14] that had been previously observed.

McClelland proposed that when two surfaces slide, the outer atoms vibrate due to the released energy. These vibrations, called *phonons*[15], travel along the surface in the form of a mechanical wave and act as a physical obstacle for the sliding interfaces. Then, wearless F_f is the necessary force to overcome the mechanical *phononic* wave, which eventually is dissipated as thermal energy. An interesting implication of this model is that the frequencies of the generated *phonons* play an important role: if the two surfaces resonate, F_f increases dramatically due to the consequent vibration amplitude enhancement. Furthermore, the *phononic* theory predicted a much more striking fact: if the *phononic* resonance between the two sliding bodies can be minimized and in the absence of wear phenomena, F_f will virtually drop to 0, which is the ultimate Holy Grail of tribologists. No more lubricants, just fine tuning the *phononic* resonance to obtain outstanding performance. Nevertheless, there were still some questions to be asked that would place the *phononic* friction as a partial explanation of the whole sliding process.

The development of Atomic Force Microscopy (AFM)[16] let McClelland and his colleagues to test their theories. Briefly, AFM consists on a micro fabricated probe ended with an extremely sharp tip that scans the sample, establishing an apparent A that can be in the nanometer range. McClelland tested his wearless friction theories just to find out that something was absolutely wrong; first of all, F_f was independent of F_v, which was in flagrant contradiction with all the previous theories. Besides, the shear stress (F_f/A) was incomprehensibly high. Quartz Crystal Microbalance measurements (QCM)[17] performed by Jacqueline Krim observed another striking effect: F_f between noble gases and metals increases a lot in the presence of liquid[18]. Far from being an intuitive idea, as liquid are commonly believed to reduce friction, it fits acceptably well with the previous thesis about high F_f between commensurate surfaces; in fact, any liquid can be reasonably commensurate with a substrate due to the weak bonds between their molecules and its fluidity. Then, the liquid lets the two surfaces in contact to match more properly, as depicted in Fig. 3. This kind of experiments explored the nature of another proposed kind of interaction: the electronic friction[19-23], arisen between the sliding

surfaces due to the electrical surface charges in the two bodies. Despite these promising developments, nor QCM experiments nor the *phononic* theory did not provide an answer for the static friction, which was still an unfathomable mystery. As an alternative explanation, it was proposed that contamination could be responsible for the presence of static friction[24]. Tribologists, who were still adapting from the macroscopic measurements to the nanoworld, really had to care about the presence of hydrocarbon molecules or water on top of the sliding surfaces and learn not to underestimate their effect on the commensurability phenomena between the sliding surfaces, the formation of adhesive bonds, the modification of the electronic interfaces which could eventually lead to a variation in electronic friction and so on.

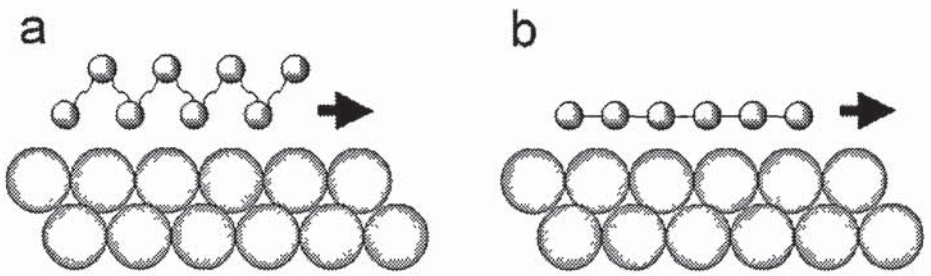

Fig. 3. *Phononic* friction. a) liquid layer sliding on a solid surface. Due to the low interaction between liquid molecules, it is easy for them to commensurate with the solid substrate and increase F_f. b) Solid layer sliding on the substrate. The sliding layer cannot keep track with the substrate interatomic distance and slides with low F_f.

Bottom line: there seems to be an insurmountable gap between macroscopic and nanometric friction. The friction laws that Leonardo came up with do not seem to apply when it comes to explain a nanometric contact. Nevertheless, there was also a giant leap from Newton to Böhr and today nobody questions the validity of quantum mechanics. Fortunately, the development of tools to explore the nanomechanics of interfaces in the nanometric scale is helping us to unveil the mysteries that connect the macroscopic and nanometric worlds.

Chapter 3

3.Atomic Force Microscopy

3.1 A NEW WAY TO STUDY SURFACES

The AFM is perhaps the most versatile member of the expanding family of Scanning Probe Microscopies (SPM). These devices have the ability to sense the surface of a sample in a wide variety of ways (mechanically[25,26], electrically[27-29], magnetically[30], etc.), offering the possibility to explore all kind of surface properties[31-34]. SPM was developed in the early 1980's when Binnig and Rohrer revolutionized microscopy through the invention of the Scanning Tunneling Microscope (STM)[35], which measures the tunneling current between two very close conductive samples and uses this current as a feedback signal so as to track the sample topography. The most important advantage of this group of techniques is the nanometric resolution they can achieve and its nearly non-destructive interaction with the sample. The fields of application of these techniques range from materials science[36,37] to physics[38,39], although in the last years AFM[16] has become an extremely useful microscope to biologists[40]. Soft films, cells and tissues have always been difficult to image in their natural liquid environment and now they can be tested in-situ[41], not only to obtain topographic information, but also from a nanomechanical point of view[42]. A new research field opens broad.

3.2 AFM. HOW IT WORKS

The operating principle of the AFM is very simple; it is based on a very thin cantilever with a sharp tip that contacts the sample of study. Then, the cantilever

senses the interaction forces that are established between the probe and the sample, namely van der Waals[43,44], electrostatic[43,45] and electronic repulsion[46] due to intimate contact between the two bodies[47]. I guess this is the moment to say that while you are working at the nanometric level, the macroscopic concept of contact must be redefined and the exact interaction forces between the approaching surfaces must be considered really carefully. Nevertheless, and for the sake of simplicity, I will keep on talking about "contact" when the tip and the sample get really close. Then, when the probe contacts the sample, the cantilever bends upwards while a certain F_v is applied to the sample. This deflection is transformed into an electric signal, which is processed and delivered as topographic information of the point where the tip is placed. While the tip has the ability to scan the surface, a topographic image of all the scanned area is obtained. A simplified AFM schematic is depicted in Fig. 4.

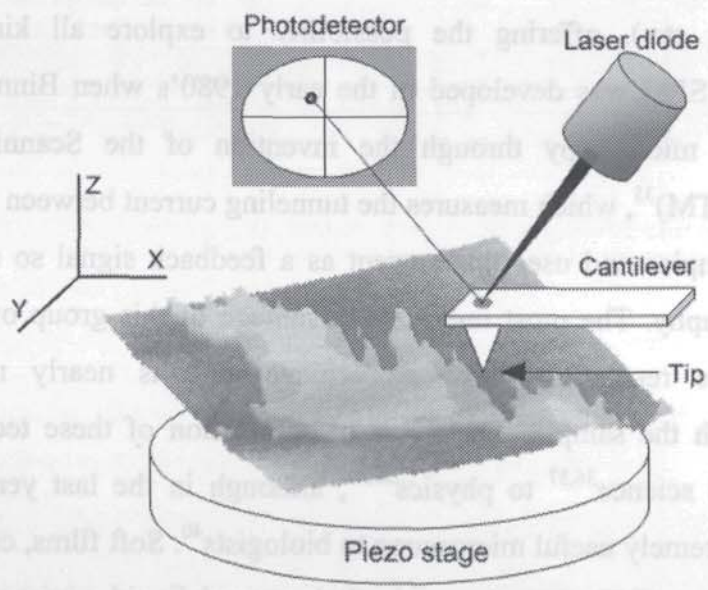

Fig. 4. Schematics of an AFM. The probe scans the sample surface, which is generally mounted on the piezo stage, in the X and Y directions. The cantilever deflection (proportional to the F_v applied on the sample) is maintained constant, and it is the piezo stage the one that moves up and down so as to keep track of the sample roughness. The system that keeps the cantilever deflection constant is a feedback loop that constantly measures the position of a laser that reflects on the cantilever back and then on the photodetector, the output of which acts as the feedback loop control signal.

3.3 AFM PARTS

3.3.1 The probe

The probe consists of a micro-fabricated, extremely sharp tip mounted at the end of a cantilever with a typical length of 50-200μm[29,48]. The tip apex, which is the part of the probe that contacts the sample, has an initial radius (*R*) that ranges from 5 to 30nm[49].

There are two basic cantilever shapes, as seen in Fig. 5:

Triangular geometry. Usually made of Si_3N_4, they have a wider back-plated zone, so it is easier to focus the laser on it. They are suitable for Lateral Force Microscopy (LFM) measurements and for liquid operation. Due to the transparency of Si_3N_4, they are usually covered with an Au layer to improve the amount of laser light reflected on the back of the cantilever. Usually, a Cr layer is deposited prior to the gold coating to improve the adherence of the reflective layer.

Rectangular geometry: easier to fabricate. Suitable for air imaging and LFM in air. They are usually made of SiO_2.

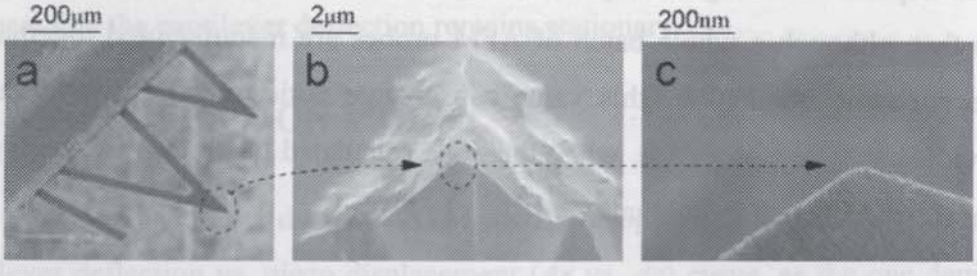

Fig. 5. a) Si_3N_4 triangular and rectangular cantilevers mounted on the same chip. b) Zoom of the tip. c) Zoom of the tip apex, with a *R* around 50nm.

Depending on the sample topography, the tip aspect ratio, that is, the ratio between the total tip length and its central width is an important parameter. In order to perform accurate height measurements in trenches it is necessary to use a high aspect ratio tip (Fig. 6), while for standard measurements or flat surfaces, a low-

aspect ratio tip is enough. Nowadays, lots of different specific tip shapes can be micro fabricated to meet specific application demands. For example, tipless cantilevers are useful for attaching colloidal probes and controlling the contact area with more accuracy[50], flat-punch tip apex can be useful for performing mechanical measurements on cells[51] and extremely thin tip apex (~1nm) are mandatory for high resolution topographic measurements[52].

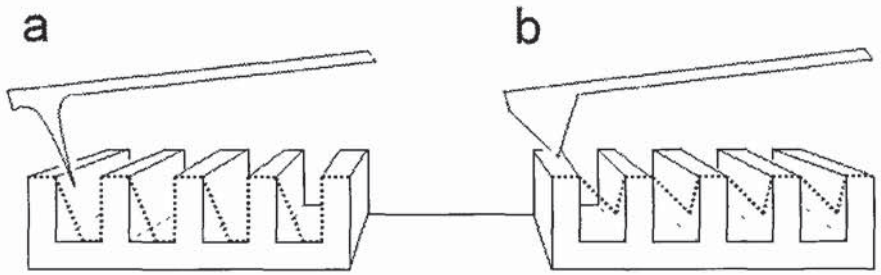

Fig. 6. a) High-aspect ratio tip, suitable for imaging deep trenches. Notice that, although this tip accurately measures the trench depth, it does not track its shape exactly. Consequently, choosing the correct tip for each job is extremely important. b) Low-aspect ratio tip, which measures both an incorrect trench depth and shape. The dotted lines in both figures mark the topographic image recorded by each tip while the solid lines are the real trench shapes.

In order to calculate the F_v exerted by the tip on the sample, the cantilever is modeled as a spring. Then, each cantilever has an elastic vertical constant (k_v) which depends on the geometry and composition of the probe. It is important to note that, although a whole batch of AFM probes are manufactured together and have the same nominal k_v, this value can change noticeably from individual to individual. As a consequence, when the F_v is calculated quantitatively, each probe k_v must be calculated individually.

3.3.2 Detectors

The most common detector for cantilever deflection is the laser beam. First of all, the laser must be micro positioned so as to impact in the back-plated surface of the cantilever and then on the photodetector. Then, when the tip deflects during scanning due to the topography of the sample, this movement is received by the photodetector as a laser spot displacement. In other words, the detector converts the

mechanical movement of the cantilever into an electric signal in the photodetector. The simplest photodiodes have two segments, so they can transmit vertical information of the tip deflection. If there are four segments, lateral deflection of the tip can also be sensed, so LFM is allowed. The signal received by the detector is sent to the feedback electronics, which maintains a constant deflection. Depending on the nature of the signal processed by the feedback loop, there are several AFM modes of operation, the most common of which will be reviewed in this section.

3.3.3 Piezoelectric

The piezoelectric fulfils two important tasks; first of all, it is responsible for the scanning movement in X-Y axes with nanometric resolution. Secondly, it moves the sample in the Z axis as a response to the sample topography. Piezoelectric materials expand or contract in a very reproducible and controlled way as external voltages are applied to them, so they are useful to create motion in a nanometric level[53-55]. Nevertheless, piezoelectric scanners hysteresis has to be assumed, although this behavior can be negligible for small scanning areas. Another fact is that piezo scanners can be susceptible to creep[56], which is a sort of relaxation that occurs under constant stress, although this problem can be detected and solved. Usually, the piezo is set beyond the sample, so it is the sample that moves while the cantilever deflection remains stationary.

3.4 AFM OPERATION MODES

To understand the different AFM modes of operation it is useful to show a cantilever deflection vs. piezo displacement (Δx vs. Δz) curve, as the one depicted in Fig. 7. This kind of representation will be discussed all along this work, as is the basis the nanoindentation experiments presented in this thesis. Basically, it consists on a vertical displacement of the cantilever towards the sample, that is, a classical indentation experiment but in a nanometric range[57]. As the cantilever approaches the sample (Fig. 7*a*), contacts it (Fig. 7*b*) and deflects (Fig. 7*c*), different force regimes can be detected. First of all, as the tip is far from the surface, there is no

interaction between the cantilever and the sample, so no Δx is detected (the cantilever deflection is tracked as a position variation of the laser spot on the photodetector). As the distance between the two bodies decreases, several interactions, namely Van der Waals, electrostatic and capillarity forces[58]) begin to build up and the cantilever bends suddenly and contacts the surface, process commonly known as *jump-to-contact*[59,60]. As the cantilever keeps on moving downwards, the electronic repulsion between the atoms of the tip and the sample becomes dominant and bends the cantilever upwards, in what we may consider as real contact or, at least, contact in the macroscopic sense.

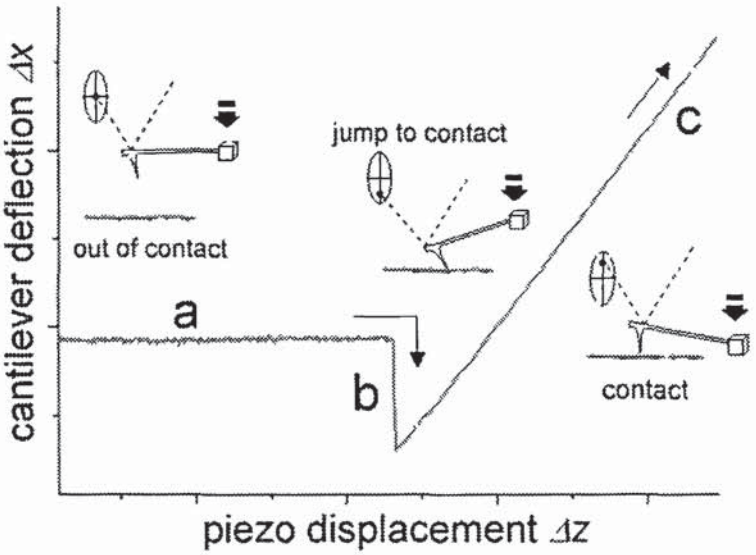

Fig. 7. Δx vs. Δz curve performed with an AFM that exemplifies the different contact regimes the tip-sample interface undergoes as both bodies approach. a) The tip is far from the surface, so there is no interaction between the two bodies. b) As the tip approaches the surface, the tip bends downwards due to attractive interactions as van der Waals, capillarity or electrostatic forces. c) Due to the hard-contact between the sample and the surface, the tip bends upwards. As the feedback loop is disconnected during the recording of Δx vs. Δz curves, the Δx can be obtained as the raw photodetector output.

3.4.1 Topographic modes

3.4.1.1 Contact mode

In this mode, the tip scans the surface while the sample and the tip are in real contact, that is to say, the cantilever is bent upwards up to a certain extent. In order to acquire a topographic image, feedback electronics processes Δx and controls the piezo stage so as to maintain a constant Δx and F_v value (Fig. 8*a*). This mode offers the best topographic resolution as the tip truly tracks the surface profile but the F_v applied by the tip can physically modify the sample and change its topography and surface properties. As a consequence, this mode is adequate to scan hard materials as metals, oxides, minerals and certain polymeric structures. When it comes to biological samples it can be used but it is extremely important to minimize the F_v exerted on the surface. Nowadays, probes with k_v values ranging from 300 to 0.01 nN/nm are commercially available, so we may want to use cantilevers with a low k_v to image soft samples.

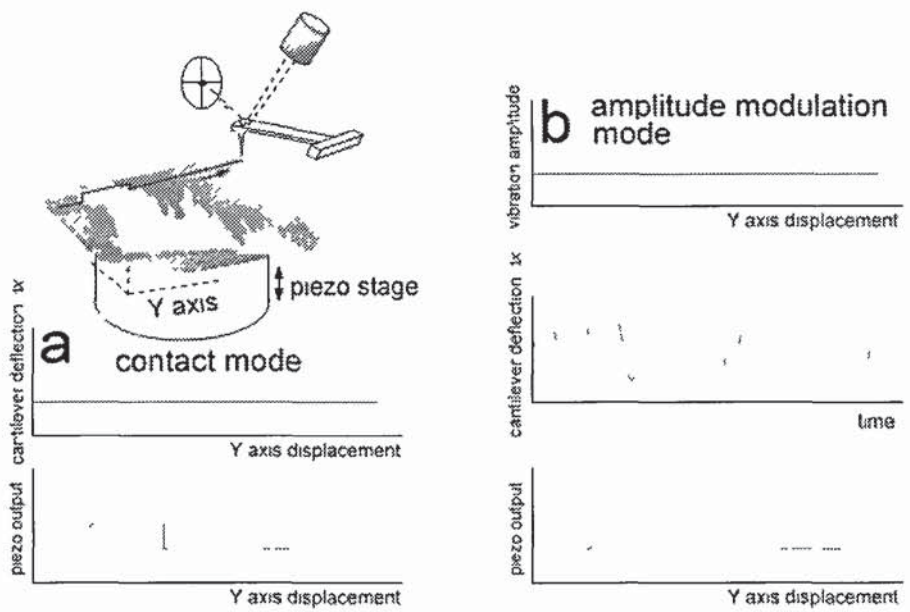

Fig. 8. The two classic modes of topographic AFM operation: contact and amplitude modulation mode. a) In contact mode, the feedback loop keeps Δx constant while the piezo output responds to the sample topography. b) In amplitude modulation mode, the cantilever oscillates at its resonance frequency. The feedback loop maintains the vibration amplitude constant, while the piezo response is the topographic signal.

3.4.1.2 Amplitude Modulation (AM-AFM) mode

In this mode the tip is forced to vibrate in its own resonance frequency by means of a small piezoelectric mounted on the cantilever holder. Then, as the tip approaches the surface, the vibration amplitude is reduced because of the interactions between probe and sample[61,62]. The electronics uses the vibration amplitude as the feedback signal to maintain a constant distance from the surface[63]. Nevertheless, we must point out that AM-AFM mode is not a truly non-contact technique[61,64], as it has been demonstrated that the tip randomly jumps from non-contact to contact regimes[65]. For the sake of simplicity, truly non-contact techniques will not be discussed here, but they have been developed in the last years and nowadays are available in a variety of commercial AFMs[66].

The AM-AFM mode has poorer resolution than contact mode because the distance between the tip and the sample is larger and, consequently, the interaction is weaker. Nevertheless, artifacts are reduced and the sample degradation due to mechanical contact is minimal, so this is a suitable mode to image soft organic surfaces.

3.4.2 Force Spectroscopy

As the AFM evolved from the original designs, further capabilities were added to the topographic operation modes. Force Spectroscopy is perhaps the most straightforward, as no additional electronics has to be added to the basic AFM controller. As we have seen, the feedback loop maintains a constant Δx while obtaining topographic images, both in contact and in AM-AFM mode; in the spectroscopic mode, the feedback loop is disconnected and the cantilever is moved towards the sample surface a certain distance Δz while Δx is recorded, as shown in Fig. 7. After the approaching process, the cantilever retracts to reach the initial rest position. Consequently, this mode lets us perform nanomechanical measurements on all kind of samples[67,68] applying F_v values that go from the mN to the pN range, depending on the AFM probe. The study of Δx *vs.* ΔZ curves can shed light on the

elastic and plastic properties of materials[69], as these curves are similar to the classical macroscopic indentation experiments, although AFM measurements imply a nanometric *A*. In the experimental section several applications and results obtained with this technique will be discussed in detail. Nevertheless, in order to exemplify all the experimental steps and calibration procedures necessary to reach quantitative results, we will discuss a Δx *vs.* Δz curve (also called force curve) example in this section. In Fig. 9, we can see a Δx *vs.* Δz curve performed on a phospholipid bilayer, which is a kind of sample thoroughly studied in this thesis. When the tip is far from the surface there is no Δx, as there is no interaction between the bilayer and the tip (Fig. 9*a*). Then, when both bodies contact, Δx increases, and the bilayer is compressed (Fig. 9*b*). This regime is broken by a discontinuity which corresponds with the bilayer puncturing[70,71] and after that, the tip contacts the mica surface and keeps deflecting until the piezo stops its motion (Fig. 9*c*). The Δx *vs.* Δz curve gives us all this information (Fig. 9d) but there are some questions that are still unsolved and that can be extracted from our experimental data:

- *Which is the F_v needed to puncture the bilayer? In other words, how much F_v the tip must apply to reach the discontinuity related with the bilayer rupture?*
- *Which is the sample penetration depth (P_d) during the sample compression and the bilayer rupture?*
- *Which are the interactions that arise between tip and sample prior to the real contact? Van der Waals, electrostatic forces, etc.*

As we can see, this information is really important to characterize the mechanical properties of the sample and its behavior while being compressed.

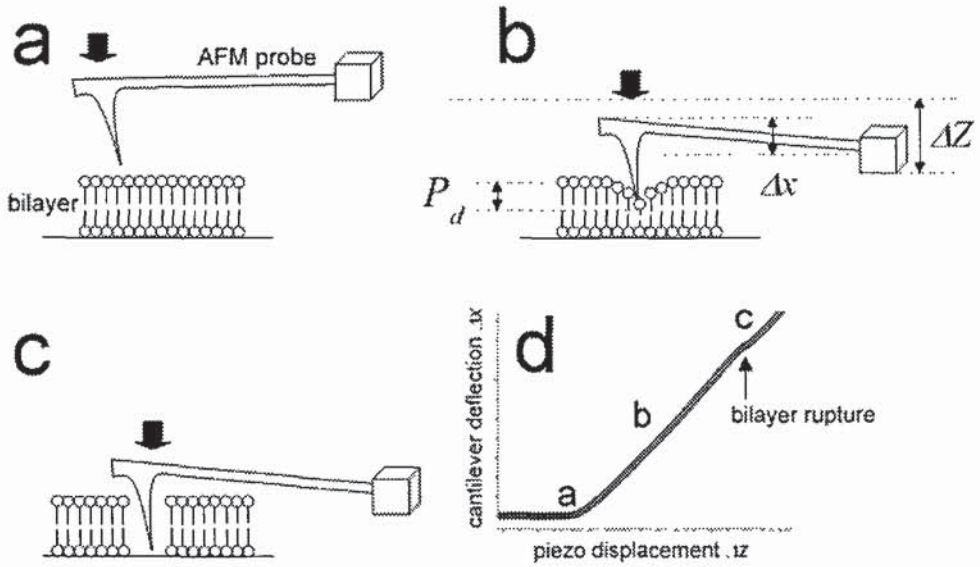

Fig. 9. Force Spectroscopy experiment (Δx *vs.* Δz curve) on a phospholipid bilayer. a) As the cantilever moves downwards, the tip contacts the sample surface. b) From the contact position the tip keeps on moving downwards (Δz), with the consequent Δx and P_d. For compliant samples, $\Delta z = P_d + \Delta x/S_v$. For non-deformable samples, $\Delta z = P_d$. ($\Delta x \sim 0$). c) The bilayer breaks and the tip contacts the substrate. d) Experimental Δx vs. Δz curve where a), b) and c) processes are marked.

3.4.2.1 F_v vs. Δz curves

To answer the first question we must relate Δx, which is the photodetector signal variation when the cantilever bends, with the real cantilever deformation (nm) while the Δx *vs.* Δz curve is performed. Besides, we must find the cantilever k_v to convert Δx into F_v.

When the tip and the sample are in contact,

$$\Delta z = P_d + \frac{\Delta x}{S_v} \tag{4}$$

Where S_v, which is the so-called vertical sensitivity, is the relationship between the signal variations in the photodetector as the cantilever deflects a certain amount. If the sample is extremely hard in comparison with the cantilever (e.g. mica or SiO_2 surface), $P_d \sim 0$ and then

$$\Delta z = \frac{\Delta x}{S_v} \tag{5}$$

S_v is the slope of the contact region of a Δx vs. Δz curve performed on a rigid substrate and is given in V/nm. Then, it is clear that

$$F_v = \frac{\Delta x}{S_v} k_v \tag{6}$$

3.4.2.2 Vertical calibration of AFM tips. Searching for the real k_v

AFM cantilevers are considered to behave as springs, assumption that is only valid for moderate Δx values, as deviations can occur at very high deformations. Nevertheless, the approximation is suitable if we consider that the deflection has to be followed by a laser that reflects on a photodetector and that this photodetector has a finite range of operation, as it is shown in Fig. 10. In fact, the most common source of error is the non-linearity of the photodetector when the laser reflects far from the center, so it is useful to check this issue prior to begin the Force Spectroscopy experiments. Photodetector non-linearity is not critical if only topographic measurements are performed with the equipment, as they are not affected by the detection system assuming that quantitative F_v values are not required.

Several methods have been implemented to experimentally measure AFM cantilevers k_v. Sader et al. proposed a method that has into account the geometry of the cantilever and its density[72]. Nevertheless, as cantilevers are structures usually conformed by layers of several materials (usually a Cr and an Au layer are deposited on the cantilever back to improve laser reflection, conductive cantilevers can have different metallic coatings[73,74], etc.), the error in the density estimation can be high. Besides, the thickness of the cantilever has to be experimentally measured, which is experimentally difficult. Further improved models use the cantilever resonant frequency and its Q factor[75,76] as parameters, so density and cantilever thickness measurements are not necessary[77]. Unfortunately, these calculations are

valid for rectangular cantilevers and in order to apply them to triangular cantilevers it is necessary to have a chip with both triangular and rectangular shaped cantilevers together and assume that the thickness of all of them is constant.

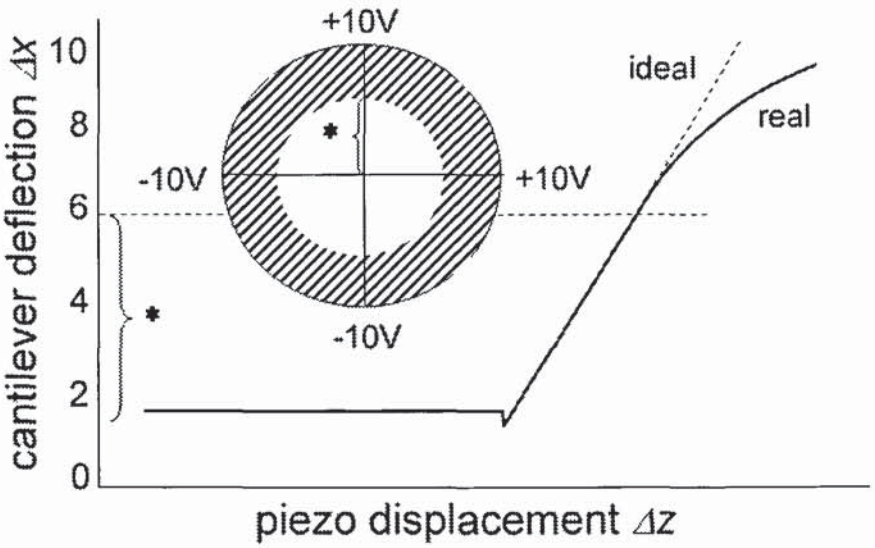

Fig. 10. Δx vs. Δz curves can be used to check both the linearity of the photodetector and the assumption that the cantilever behaves as an ideal spring, that is, that Hook's law can be applied to model its behavior. This imaginary photodetector with a range of ±10V in vertical and lateral axes is linear in the region ±6V if radial symmetry is assumed (non-linear region is stripped in the photodetector cartoon and the linear region in the vertical positive axis is marked with a * both in the Δx vs. Δz curve and in the photodetector). As a result, no quantitative measurements can be obtained in the stripped region.

Cleveland et al. proposed to measure the cantilever resonance frequency shift as a mass is added to the cantilever to calculate the k_v[78]. Practically, tungsten micro spheres are deposited on a glass slide and picked up by the cantilever by capillarity forces. The distance between the free end of the cantilever and the added mass has to be accurately measured because it strongly influences the resonance frequency shift. The most important handicap of this method is that it is difficult to calculate the mass of the attached micro spheres because of the indetermination in the material density and the deviation from the spherical shape.

If a reference cantilever with a known k_v is available, other cantilevers can be vertically calibrated. The technique consists on pushing the reference cantilever with the uncalibrated one. Measuring Δx while knowing Δz once the two cantilevers

are in contact gives an accurate measurement of the vertical force constant[79]. A recent work has been devoted to compare all the reviewed calibration methods, point out the experimental problems of each one and their advantages respect to the others[80].

The method that we have used to vertically calibrate the cantilevers is called thermal noise[81,82]; it is based on the measurement of the thermal spectrum of the cantilever, which is approximated to a simple harmonic oscillator[83]. Within this model, once the parameters have been set up for the thermal spectrum, the spring constant is obtained from the equipartition theorem:

$$\Delta F = \sqrt{\frac{4k_b TBk_c}{\omega_0 Q}} \tag{7}$$

Where ΔF is the RMS amplitude of the force noise, k_b is the Boltzmann constant, T is the temperature, B is the measurement bandwidth and ω_0 is the free cantilever resonance frequency.

The thermal noise method is valid for beam shaped and triangular probes, although it is not suitable for stiff cantilevers ΔF is too small to be detected. Between its drawbacks we can find that the obtained F_v varies significantly depending on the laser position on the cantilever and on the medium where the measurements are performed (air, water or vacuum)[84].

3.4.2.3 F_v vs. P_d curves

F_v vs. P_d curves give us information about the whole deformation the sample undergoes as it is compressed. In the present work, these representations have been extensively used to experimentally measure the sample thickness, as this value must equal the total P_d after completely puncturing the sample. F_v vs. P_d curves also provide information about the different elastic and plastic deformations the sample undergoes while being compressed. As an example, our work with alkanethiols on gold demonstrates how these molecules fold in a sequential way as F_v increases, how much F_v must be applied to trigger these molecular foldings and

the monolayer thickness diminution after each of these events takes place (section 4.6.3).

Considering that,

$$P_d = \Delta z - \frac{\Delta x}{S_v} \tag{8}$$

Now we have got all we need to go from Δx *vs.* Δz curves to F_v vs. Δz curves to F_v vs. P_d curves. Just as a summary of the whole process from the Δx vs. Δz curve to the F_v vs. P_d curve, the different fore representations are depicted in Fig. 11, where the change of the curve shape after the mathematical treatments can be seen.

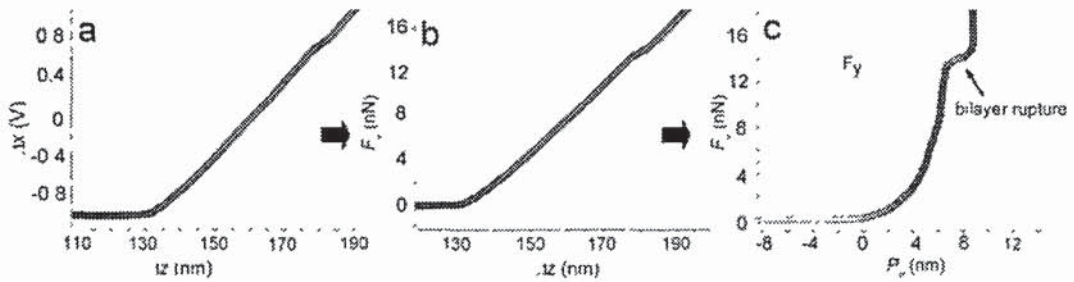

Fig. 11. Evolution of a Δx *vs.* Δz curve performed on a phospholipid bilayer in liquid environment as obtained from the AFM towards a fully meaningful representation. a) Δx vs. Δz curve (raw AFM information). b) By means of k_v and S_v and applying equation 6, F_v vs. Δz can be obtained, which provides quantitative force information. c) F_v vs. P_d curve, where both the F_v at which the bilayer breaks under compression (F_y) and the P_d of the rupture event can be calculated.

3.4.3 Lateral Force / Friction Force Microscopy (LFM). A tool for nanotribologists.

LFM is a technique derived from contact AFM that is used to obtain the friction properties of surfaces in the micro- to nanometric range[85-87]. In order to perform the measurements, the tip scans the sample in a direction that is

perpendicular to the cantilever long axis, bending the cantilever laterally (Fig. 12*a*). This lateral bending (Δy), which is proportional to F_f, is detected by the photodetector (a four quadrant photodetector is needed: the difference in light intensity between the two upper and lower quadrants is used to determine Δx, while the difference in light intensity between the left and right quadrants stands for the cantilever lateral deflection).

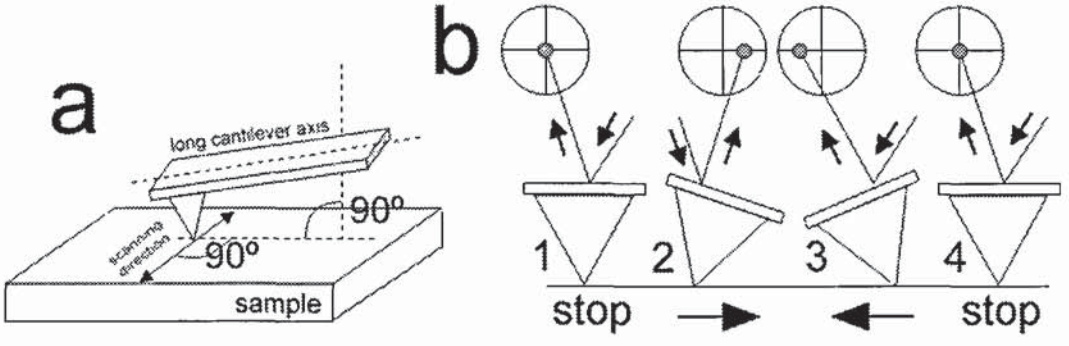

Fig. 12. LFM operation. a) The tip scans the surface perpendicularly to the main cantilever axis. b) Whole friction measurement (friction loop): 1 - the cantilever stands still on the surface. 2 – the tip scans the sample from left to right, creating a cantilever torsion that is detected by the photodetector. 3 – the same process but scanning from right to left. Now the laser spot is in the left side of the photodetector. 4 – end of the loop.

To obtain the F_f value in a certain area of our sample, a friction loop has to be acquired, which means scanning a line from right to left and then from left to right (Fig. 12*b*). The total friction energy dissipated during the scanning process is proportional to the area of the loop (Fig. 13) and the average F_f in the scanned line is

$$F_f = |F_f(\text{left-right}) - F_f(\text{right-left})| / 2 \qquad (9)$$

The most straightforward application of LFM is obtaining contrast in samples with different domains[88-90]. As the tip scans the surface, Δy value changes according to the mechanical properties of the scanned areas. This mode can be really useful when domains with different composition/structure but similar height can not be discriminated by means of topographic AFM[91].

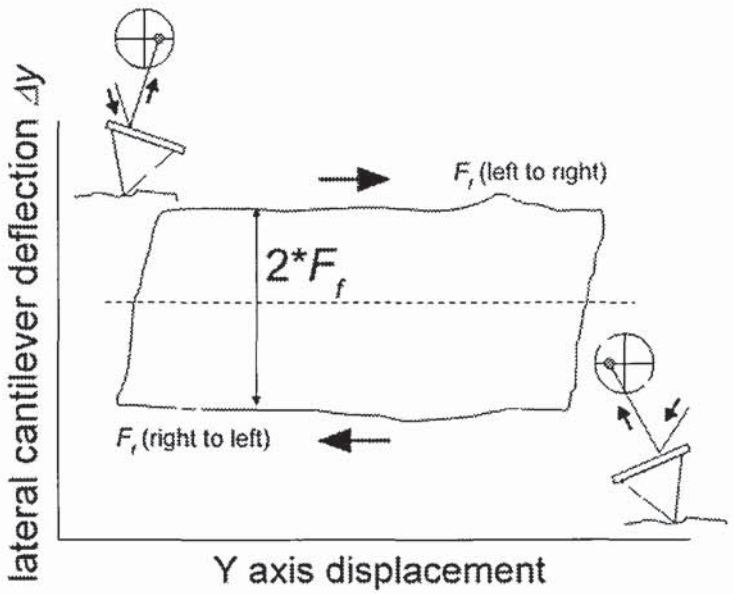

Fig. 13. Δy vs. Y axis displacement while a friction loop is performed. The area of the loop is proportional to the total energy dissipated during the process and F_f in a certain position is proportional to the half width of the friction loop, as expressed in equation 9.

But we can move a step further and try to obtain quantitative values for F_f. In this direction, a kind of experiment that renders extremely useful information is the so-called F_f vs. F_v spectroscopy, which consists on a gradual increase of the F_v applied on the sample as the F_f value is recorded[92]. This way, we obtain a complete nanotribological test over the range of F_v values we are interested in. Moreover, if we go back to our undergrad friction knowledge,

$$F_f = \mu F_v \tag{10}$$

μ can be also obtained if we can get quantitative values for F_v and F_f. The experimental setup to perform this kind of measurements is depicted in Fig. 14. Unfortunately, it must be said that in the nanometric range the relationship between F_v and F_f it is not always as simple as that[93] but it keeps on working for a wide variety of materials[94,95]. As it was shown in the Force Spectroscopy section, quantitative values for F_v can be obtained if S_v and k_v are known. To obtain reliable values for F_f, the cantilever must be laterally calibrated, that is to say, the relationship between Δy and the real F_f must be established.

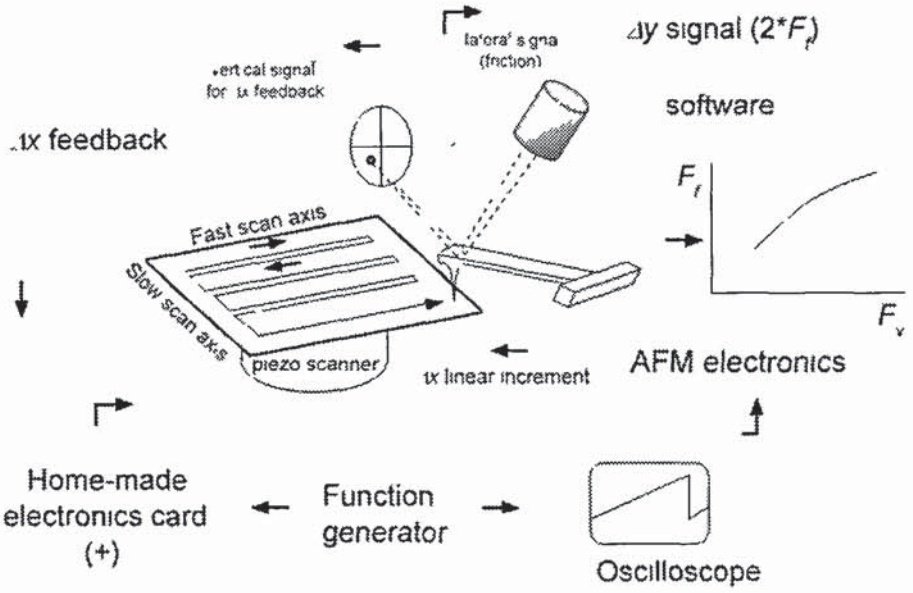

Fig. 14. LFM experimental setup to obtain F_f vs. F_v curves. As the tip scans the sample at a certain F_v, Δy is recorded. At the same time, feedback controls Δx value (proportional to F_v). In order to increase F_v in a linear way, a saw-tooth function is injected to the Δx feedback electronics through a home-made electronics card. The resulting signal is used to move the piezo scanner in order to vertically deflect the cantilever and match the new Δx feedback value. This way, the F_f is recorded simultaneously to the applied F_v.

3.4.3.1 Lateral calibration of AFM tips. The long way to obtain quantitative F_f measurements.

Several methods have been proposed in the past to find cantilever lateral constant (k_l) and lateral sensitivity (S_l). Green et al. extended Sader's geometrical method to find k_v also to calculate k_l, as well as Cleveland did for its added mass method[96]. Liu et al.[97] proposed a method concerning the calibration of the lateral response of the photodetector as a function of the torsion angle of the cantilever while performing the friction measurements and Cain et al.[98] analyzed the static friction arisen between tip and sample in order to infer the mechanical constants of the cantilevers. Although studies comparing these methods demonstrate that they are consistent and render quantitative values[99], perhaps the method proposed by Ogletree et al.[100] is the most widely used and it has also been the method used to laterally calibrate our cantilevers.

3.4.3.1.1 Wedge calibration method

When a sloped surface is scanned, several forces arise in the point of contact between sample and tip, as depicted in Fig. 15*a* and *b*. The F_v exerted by the tip on the sample can be decomposed in two perpendicular contributions, that is, the load (L) and the tractive force (T+ or T-, depending on the scan direction). These forces are counteracted by the surface, which applies a normal force (N) which is parallel to the tip axis (F_v) and a F_f perpendicular to F_v and opposite to T. It is interesting to note that this equilibrium is only valid when the two surfaces slide, but not during static friction, where T value is lower than F_f and the two bodies do not change their relative position respect each other. The cited equilibrium can be written as

$$\begin{aligned} F_v &= L\cos\theta \pm T_{\pm}\sin\theta_t \\ F_f &= T_{\pm}\cos\theta \pm L\sin\theta_t \end{aligned} \tag{11}$$

Where θ_t represents the surface inclination. $T\pm$ value is proportional to the Δy value, being S_l (in N/V) the proportional factor:

$$T = S_l * \Delta y \tag{12}$$

It is important to note that several factors will modify the S_l value. First of all, S_l is dependent on the position of the laser on the cantilever back and also on the position of the photodetector. In the vast majority of commercial AFM systems, the photodetector physical movement is coupled between the X and the Y axes, so when it moves in one axis, the laser spot also moves in the other. This effect can be due to a misalignment of the laser path respect to the photodetector or because of a mechanical coupling of the screws that move it. In all cases, moving the photodetector changes S_l and, consequently, the validity of the calibration. This effect can be a major problem when compliant tips are used (0.01-0.1N/m) because the laser position on the photodetector can derive importantly with time and also with humidity. Of course, AFM probes with different k_v will have different S_l values but AFM tips coming from the same batch will also differ in this value. Again, the same tip can have different S_l values depending on the laser position and

the photodetector, so once the cantilever is laterally calibrated NOTHING concerning the laser path or tip position can be modified. This is extremely important because otherwise aberrant results can be obtained.

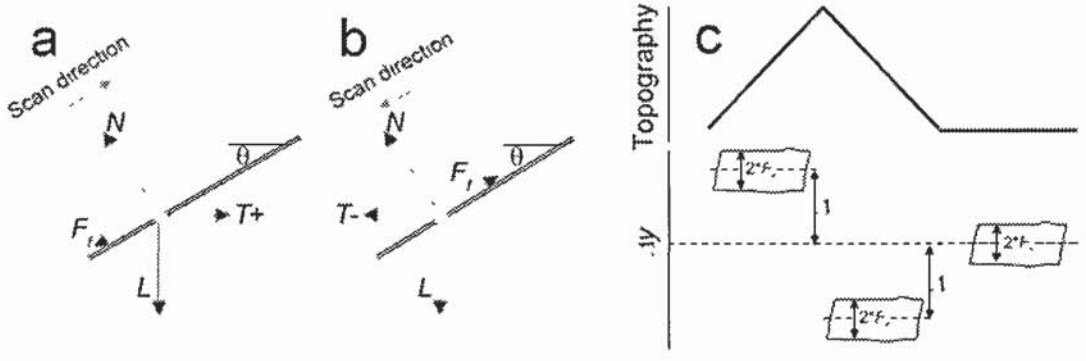

Fig. 15. a) and b) Balance of forces while the tip scans a slopped surface. The F_v exerted by the tip is decomposed in two components: a load (L) and a tractive force (T+ and T-). These forces are counteracted by the normal force exerted by the surface on the tip (N) and F_f. c) Δy signal as friction loops are performed on differently slopped surfaces. The width of the friction loop ($2*F_f$) is independent of the slope angle but the whole friction loop moves upwards or downwards an offset value (Δ) depending on the surface inclination.

Let's go back to the S_l calculation method. To do that, we must introduce adhesion (A_d) as a new force. When the relationship between F_f and F_v is linear, A_d is considered as an additive term to F_v:

$$F_f = \mu(F_v + A_d) \tag{13}$$

So it is verified that

$$F_{v+} = \frac{L + \mu A_d \sin\theta_t}{\cos\theta - \mu \sin\theta_t} \tag{14}$$

$$F_{v-} = \frac{L - \mu A_d \sin\theta_t}{\cos\theta + \mu \sin\theta_t} \tag{15}$$

Being F_{v+} and F_{v-} the vertical force values in opposite scanning directions and θ_t the sample slope angle. As we can see, F_v strongly depends on θ_t and also on the sliding direction.

The width of the friction loops does not depend on θ_t, so it will remain the same independently of the scanning direction. It must be pointed out that this is true when the sample is homogeneous in a chemical and structural sense: if there are different sample-tip interfaces while scanning up or downhill, then F_f differences will rise for sure. Nevertheless, the position of the friction loop in the photodetector will change a certain offset value (Δ) as it can be seen in Fig. 15*c*. According to this and assuming linearity between F_f and F_v,

$$\Delta = \frac{(1+\mu^2)\sin\theta\cos\theta}{\cos^2\theta - \mu^2\sin^2\theta} \tag{16}$$

$$2F_f = \frac{\mu}{\cos^2\theta - \mu^2\sin^2\theta} \tag{17}$$

Being $2F_f$ the width of the friction loop. Δ and F_f values that we find experimentally are in photodetector volts, so

$$\Delta = \Delta_0 * S_l \tag{18}$$

$$2F_f = 2F_{f0} * S_l \tag{19}$$

Where the sub index "$_0$" corresponds to magnitudes in volts.

According to this method, scanning a sample with well-known slope angles at different F_v values is enough to find S_l. The first proposed kind of surface for this purpose was $SrTiO_3$ which, after being conveniently annealed, shows (001) and (100) crystalline faces forming sharp ridges[101]. Because of the crystalline nature of the material, the dihedral angle between ridges is extremely reproducible. The problem with this surface is that the height of the ridges can be as low as 10 nm and they are only 100-200 nm apart. Because of that, $SrTiO_3$ is not suitable to laterally calibrate blunt tips, as they cannot track the sample surface properly. In the last years, several SiO_2 calibration grids with well-characterized surface slopes are commercially available. The main advantage is that they do not need any treatment, are mechanically robust, chemically inert (at least in air and aqueous environments)

and they sport ridges that are several micrometers wide and high, being perfect for calibrating the vast majority of the commercial AFM probes. Besides, ridged calibration gratings are useful to experimentally measure the tip R; the ridges are extremely sharp (the curvature radius of the ridge top is typically less than 10 nm), so if a topographic image of the ridge top is performed with a tip sporting a $R >$ 10nm, we will obtain the tip apex profile as it can be seen in Fig. 16.

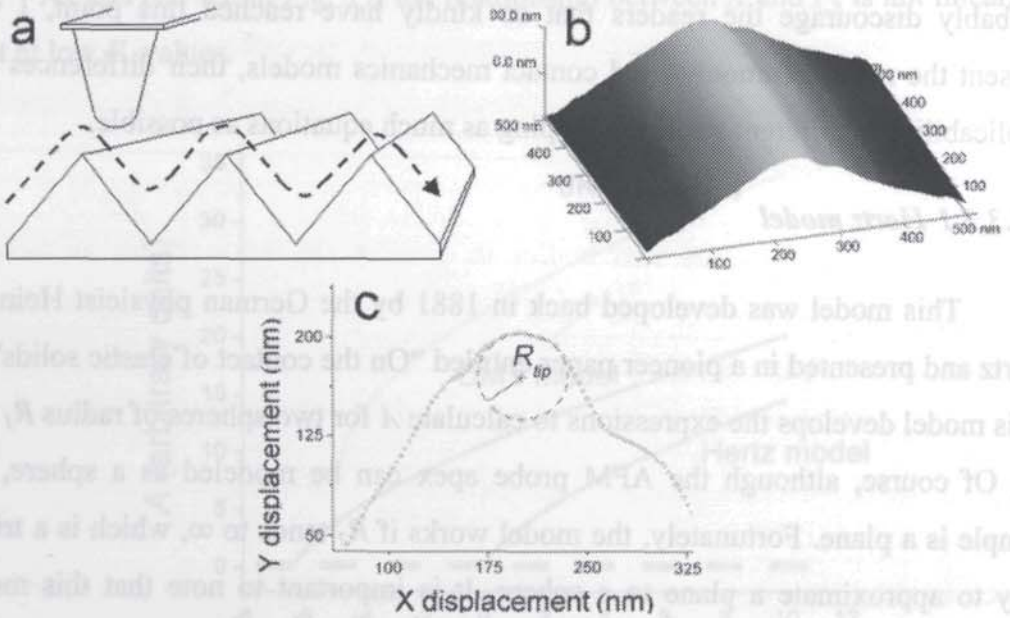

Fig. 16. Experimental calculus of the tip R. a) The tip scans the surface of the SiO_2 grid or the $SrTiO_3$ annealed sample. As the sample peaks are sharper than the tip, the topographic profile of the sample ridges is the tip apex image. b) AFM image of a SiO_2 ridge, where the peak appears blunt. C) Cross section of the AFM image, where the real tip R can be calculated.

3.4.3.2 Contact mechanics models

Due to the nanometric nature of the contacts between the AFM probe and the sample, A cannot be measured directly by any imaging technique, as it would be possible in macroscopic experiments[102,103]. Nevertheless, knowing A can be extremely important as it will give us information about how many molecules we are scanning per area unit while performing LFM experiments or how many molecules are affected when the tip indents the sample in a Force Spectroscopy test. It will be also extremely important in order to quantify the energy transferred

to every single molecule as these experiments are performed. Although the issue about the real and the apparent A is still a matter of debate, several contact mechanics models were developed in the past in order to explain interactions between bodies of different nature, being applied successfully in the macro- and microscopic world[104]. Down to the nanoworld, these models have been also applied, and I would say that obtaining a reasonable success[105]. Although an extensive explanation of these models is out of the scope of this thesis and would probably discourage the readers that so kindly have reached this point, I will present the most commonly used contact mechanics models, their differences and applicability to different surfaces skipping as much equations as possible.

3.4.3.2.1 Hertz model

This model was developed back in 1881 by the German physicist Heinrich Hertz and presented in a pioneer paper entitled "On the contact of elastic solids"[106]. This model develops the expressions to calculate A for two spheres of radius R_1 and R_2. Of course, although the AFM probe apex can be modeled as a sphere, the sample is a plane. Fortunately, the model works if R_2 tends to ∞, which is a tricky way to approximate a plane to a sphere. It is important to note that this model considers that the two spheres, as they are pushed together, do not deform plastically and that no long range interactions affect the contact.

The symmetric nature of this approach leads to a circular and flat A that can be expressed as

$$A = \pi\left(\frac{RF_v}{K}\right)^{\frac{2}{3}} \tag{20}$$

Where K is the combined elastic modulus of the two surfaces in contact,

$$K = \frac{3}{4}\left(\frac{1-\nu_1^2}{E_1} + \frac{1-\nu_2^2}{E_2}\right)^{-1} \tag{21}$$

And E_1 and E_2 are the Young's moduli of the two surfaces in contact and υ_1 and υ_2, their Poisson ratios. R value in equation 20 corresponds with

$$R = \left(\frac{1}{R_1} + \frac{1}{R_2} \right)^{-1} \tag{22}$$

Where R_1 and R_2 are the radii of the two spheres in contact.

As you can see in Fig. 17, the relationship between A and F_v is not linear, at least at low F_v values.

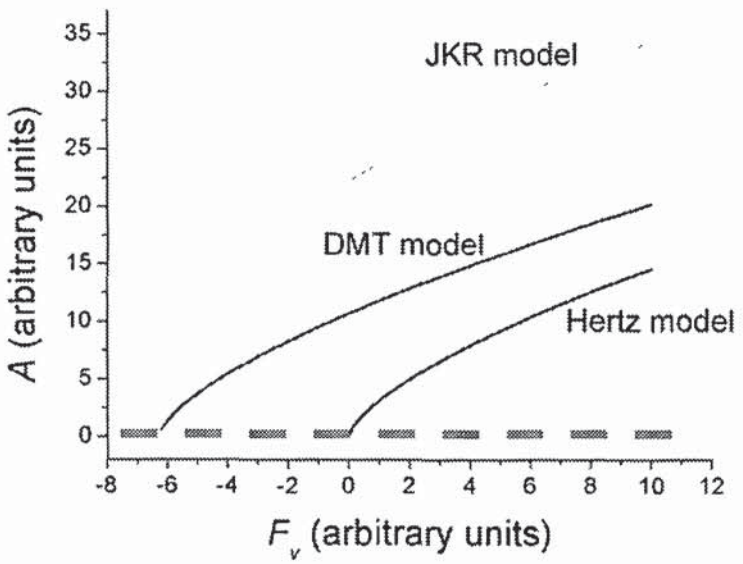

Fig. 17. Dependence between A and F_v for the most common contact mechanics models: Hertz, JKR and DMT. JKR model predicts the higher contact areas, while hertzian contact cannot be extended to negative F_v values, as it does not take into account any adhesive force.

3.4.3.2.2 JKR model

Johnson, Kendall and Roberts (1964-1971)[107-109] developed a contact mechanics model that refined the somewhat crude hertzian area of contact. They considered the energy of adhesion (γ), that is, the work per unit area necessary to separate the two surfaces in contact, to play an important role in the A calculation, where

$$\gamma = \gamma_1 + \gamma_2 - \gamma_{12} \tag{23}$$

γ_1 and γ_2 stand for the surface energies of the two contacting bodies and γ_{12} is the interfacial energy. Then, γ has into account all the attractive forces arisen between the tip and the sample. As you may expect, this model is particularly suitable for tips with a large R and for sticky surfaces, as these two factors will result in a noticeable increment of attractive van der Waals forces. Nevertheless, this model considers that the attractive interactions only take place when the two surfaces are in contact and no effect is noticed by the tip as it approaches the sample. Despite of the limitations of this model it was experimentally verified by means of SFA experiments[110].

Considering that the two bodies in contact can be modeled as spheres (although the validity of the JKR model was also extended to other geometries[108,109]), the expression for A is

$$A = \pi \frac{R^{2/3}}{K^{2/3}} \left(F_v + 3\pi\gamma R + \sqrt{6\pi\gamma R F_v + (3\pi\gamma R)^2} \right)^{2/3} \tag{24}$$

As you may note, when $\gamma \rightarrow 0$ no adhesive interactions), we obtain the expression for the Hertz model. In Fig. 17, you can see that A at a certain F_v is always higher for the JKR than for the Hertz model; well, the difference is due to the adhesive interaction, so it is really didactic to see the huge effect it can play and gives us an idea of the importance of choosing an appropriate model.

The JKR model, because of the adhesive interaction, predicts which will be the critical vertical force (F_{vc}) to separate the two bodies

$$F_{vc} = -\frac{3}{2}\pi\gamma R \tag{25}$$

And it also predicts the area of contact when F_{vc} is applied (A_c)

$$A_c = \pi \left(\frac{3\pi\gamma R^2}{2K} \right)^{2/3} \tag{26}$$

3.4.3.2.3 DMT model

The DMT model, proposed by Derjaguin, Müller and Toporov (1975)[111] takes into account the adhesive interactions between surfaces but in a different way than in the JKR theory: it considers the attractive interaction as an increase of F_v while maintaining the profile of the hertzian area of contact. As a consequence, we can consider it as a modified Hertz model, so it works well for hard substrates with low deformation rates. The advantage over the other theories is that γ is not only taken into account when the two bodies are in contact but the tip-sample interaction is shaped as a kind of Lennard-Jones potential profile.

A is expressed as

$$A = \pi \frac{R^{2/3}}{K^{2/3}} \left(F_v + 2\pi\gamma R\right)^{2/3} \tag{27}$$

Again, as in the JKR model, an expression for F_{vc} is proposed:

$$F_{vc} = -2\pi\gamma R \tag{28}$$

Because this model is based on the Hertzian theory, A_c is 0, so no *jump-off-contact* is predicted.

3.4.3.2.4 Which is the model I need?

The representation of A vs. F_v for the three presented contact mechanics models is very useful to understand the nature of each theory and to sum up the most important characteristics of each one. Having in mind the principles of Hertz, JKR and DMT theories will be really useful in order to understand how the tip contacts our sample, as this 3 models stand for limit situations. As we can see in Fig. 17, Hertz model is not useful if strong adhesive forces are present between the tip and the sample, as it does not work for "negative" F_v values. The way we have to check if there are strong adhesive forces between the tip and the sample is to perform a Δx vs. Δz curve. This time we will not focus on the approach curve but on the retraction one (Fig. 18). Then, as the tip is brought into contact and is

retracted, the tip can get stuck in the surface because of van der Waals, electrostatic and water meniscus forces. Eventually, after withdrawing the cantilever from the surface, the tip will snap off the surface in what it is called a *jump-off-contact* event. Then, the magnitude of the F_A value can be experimentally measured. Of course, F_A depends, between other factors, on the tip R. This effect is particularly important when the experiments are performed in air and water meniscus are formed between the tip and the sample, so I would suggest to perform Force Spectroscopy experiments in liquid environment (when possible); the magnitude of the water meniscus F_A usually masks all the other attractive interactions and a faithful analysis of the kind of contact is difficult to perform. Because hertzian contacts do not have into account adhesive forces, F_A at a certain F_v is always lower than in the JKR or DMT models. In this direction, JKR predicts the higher area of contact as the two bodies deform in order to accommodate the adhesive force interaction. The DMT model, as said before, is a kind of refined Hertz theory, so the bodies do not deform because of F_A. Then, it lies between the Hertz and DMT model as far as A_c vs. F_v is concerned.

If we move to the adhesive region of Fig. 18, that is, the region with negative Δx values, and apply the models, we see that the highest adhesion is predicted by the DMT model. As you can imagine by now, the A_c value is 0 because the two bodies in contact do not deform, leading to a *jump-off-contact* when A is virtually 0. On the other hand, the JKR model predicts lower F_A values but A_c is not 0 because of the deformation of the tip and the sample as F_A are taken into account.

To conclude, and having in mind that the calculation of F_A is mandatory to correctly choose a model, we will use Hertz model for hard samples or when F_A are low (when I talk about hard samples it means that they do not deform noticeably under the exerted F_v). For hard samples that present some F_A, the DMT model is more adequate. Finally, for soft samples that deform under the exerted pressure or for heavily worn tips, JKR model will be our choice.

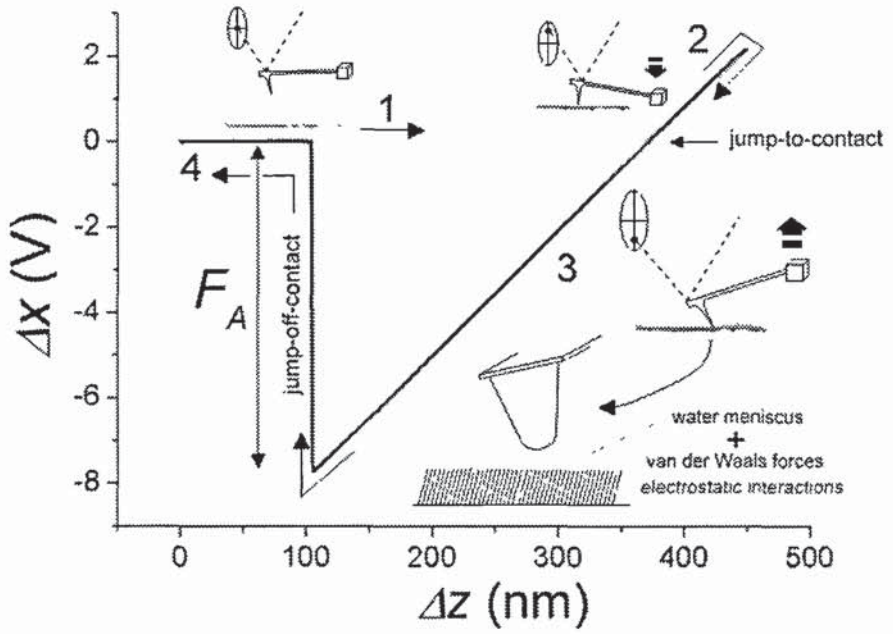

Fig. 18. Experimental measurement of F_A while performing a Δx vs. Δz curve. 1) The tip moves towards the sample surface. 2) The tip deflects upwards because of the intimate contact with the sample. 3) As the tip retracts, it gets stuck to the surface because of F_A, which results, in general, from the combination of van der Waals, electrostatic and water meniscus forces. In Δx vs. Δz curves performed in air, the water meniscus can mask all the other interactions. At a certain F_v, F_A is surpassed by the elastic energy stored in the cantilever and the tip is released (*jump-off-contact*), returning to the non-contact equilibrium position (4).

Of course, the vast majority of samples will fall somewhere between the models presented here because of their nanomechanical properties. In this direction, Rob Johnson[112], Maugis[113] and Müller[114] developed an intermediate model between the DMT and JKR theory, proposing the calculation of the so-called Tabor's parameter. The curious reader is invited to keep on studying this issue in the works of Rob Carpick, where the application of the intermediate theory is worked out and applied to friction measurements[115].

3.5 EXPERIMENTAL RESULTS

3.5.1 Nanotribology of Supported Lipid Bilayers and Langmuir-Blodgett films

J. Torrent-Burgués[a], *G. Oncins*[b], *S. Garcia-Manyes*[b], *F. Sanz*[b]

[a]Department of Chemical Engineering, Universitat Politècnica de Catalunya, Colom 1, 08222, Terrassa (Barcelona), Spain

[b]Department of Physical Chemistry, Universitat de Barcelona and Center of Nanobioengineering of Catalonia (CREBEC), Martí i Franquès 1, 08028 Barcelona, Spain

3.5.1.1 Summary

This work will be included as a chapter in the book *Biomimetics in Biophysics: model systems, experimental techniques and computation*, edited by Jose Luis Toca-Herrera (group leader in CIC Biomagune, Donosti) and published by Elsevier. We describe the LFM technique from an experimental point of view, reviewing the different setups proposed in the literature and the different calibration techniques to obtain the vertical and lateral constant values for AFM probes, as well as some hands-on tricks that we believe can be useful for scientists interested in applying LFM to their own samples. Besides, as the book is oriented towards the formation and study of monolayers, the bibliography about the nanomechanical response of these structures is reviewed, specially pointing out the results obtained on Langmuir-Blodgett films. Besides, some structural and nanomechanical concepts about phospholipid bilayers are also included, as it is an issue that we have studied extensively in our research group.

Nanotribology on Supported Lipid Bilayers and Langmuir-Blodgett films

J. Torrent-Burgués[1], G. Oncins[2], S. García-Manyes[2] and F. Sanz[2]
(1) Department of Chemical Engineering, Universitat Politècnica de Catalunya, C/ Colom 1, 08222 Terrassa (Barcelona)
(2) Department of Physical Chemistry, Universitat de Barcelona, C/ Martí i Franquès 1, 08028, Barcelona

Short title: Nanotribology on SLBs and LB films

ABSTRACT

The atomic force microscopies can be applied to the study of topographic, mechanical, chemical and reological properties of compliant materials, as cell membranes, supported planar bilayers or Langmuir-Blodgett films. The Friction or Lateral Force Microscopy, presented in section 2, is a technique derived from the Atomic Force Microscopy that permits to obtain the nanotribological characteristics and chemomechanical behaviour of nanometric films, which is usually complemented with topographic measurements and Force Spectroscopy. Biomimetic systems as supported lipid bilayers and supported Langmuir-Blodgett films of phospholipids or fatty acids have been studied with these techniques, observing the influence of factors as the pH, ionic strength or surface pressure on the properties of these systems.

1. INTRODUCTION

Phospholipids, together with proteins, are natural components of cellular membranes. Then, the study of their physical and chemical properties is very important in order to understand the wide variety of biological processes that take place across the membranes. Besides the active role that cell membranes play in cellular processes, they also act as barriers that divide the cells into compartments with different electrolytic solutions that provide specific conditions for the development of the cell biochemical reactions [1].

Supported planar bilayers (SPBs) can be used as model membranes to study cell-cell recognition, cell adhesion, phospholipid diffusion, protein binding to lipid ligands and membrane insertion of proteins [2, 3]. Atomic Force Microscopy (AFM), as a nanoscale imaging tool, is suitable to study SPBs structure but also DNA, tissues, and a vast array of biological samples and to estimate their mechanical properties. The various modes of imaging and force spectroscopies can correlate structure, properties, chemical and mechanical (chemomechanical) molecular interactions not only in air but also in aqueous environments [4-7], fact that expands AFM application fields to the study of in-situ biological processes.

Regarding the mechanics of biological samples, nanoindentation has proved to be a very sensitive technique in the micro- and nanoscale range [8]. With a typical vertical force applied on the sample that ranges from 1μN to tens of pN, AFM extends the capabilities of macroscale mechanical testings to a whole new dimension where single molecule force measurements can be performed and quantified [9]. As an example, Force Spectroscopy has allowed acquiring basic information in lipid bilayers with piconewton resolution, shedding light on the nature of electrostatic, Van der Waals and hydration interactions between molecules [10].

Friction Force Microscopy (FFM), or also called Lateral Force Microscopy (LFM), is an AFM derived technique that measures lateral forces on the atomic scale while sliding an AFM tip over the sample surface. FFM has been used for structural and technologically relevant materials [11-13], but its use has also been extended to soft and biological materials [13-15]. In this direction, frictional properties of phospholipid monolayers or bilayers on solid substrates have been studied recently [16-19], and these tribological studies have been complemented with mechanical measurements performed with other techniques [20-23].

2. FRICTION FORCE MICROSCOPY (FFM)

2.1 Atomic Force Microscopy and related techniques

Since the development of the Scanning Tunnelling Microscopy by Binnig and Rohrer in 1982 [24], several related techniques have been implemented, being the AFM the most widely used [25]. Its operation principle is simple: it consists of a probe that scans the surface of a sample and that is sensitive to its topography. The probe is a pyramidal tip mounted at the end of a microfabricated cantilever with a typical length ranging from tens to hundreds of microns. The apex of the tip is responsible for the lateral resolution of the obtained images, so its radius is in the tens of nanometers range. The deflection of the probe as the sample is scanned is usually detected by a laser that reflects on the back of the cantilever. Then, the laser position is recorded by a photodetector and injected into a feedback loop that corrects the sample position using a piezo actuator. Several modes of operation with different ways of sensing the sample surface have been implemented, being the most common the contact mode (the tip is in close contact with the surface and the electronic repulsions between tip and sample are responsible for cantilever deflection), intermittent contact mode (the tip is mechanically oscillated at its resonant frequency and sporadically contacts the sample surface) and non-contact mode (the tip oscillation amplitude is just a few nanometers and the tip is only sensitive to the attractive Van

der Waals forces arisen between tip and sample, so they are never in "real" contact). An extremely important related technique is the Force Spectroscopy, which provides nanomechanical information of the sample. Differing from AFM, the tip does not scan the surface of the sample, but stands on a certain point and compresses vertically. As the vertical deflection feedback loop is disconnected, the cantilever bends up and the representation of vertical deflection vs. Z piezo movement (force curve) can be recorded. Information about the compression properties of the sample can be obtained, besides mechanical parameters as Young's modulus. Interestingly, as the applied force is extremely low, only the outer surface of the sample is probed, so very local mechanical information can be obtained.

2.2 Friction Force Microscopy (FFM)

This technique is used to study the nanotribological properties of a wide variety of samples, and the obtained mechanical information is usually complemented with AFM measurements and Force Spectroscopy in order to obtain a whole picture of the mechanical properties of the studied material. Until now, this technique has been used to investigate the behaviour of monolayers, membranes and nanometric films, both from a purely quantitative mechanical point of view or as a tool to differentiate and contrast samples with different compositional or structural properties.

Friction and related processes can be found underlying almost any human activity. During our daily routine, we interact with dozens of machines and devices and in the vast majority of them, friction plays and important role. From this point of view, no matter to say that a deep understanding of friction and wear processes is of crucial importance in efforts to design mechanical systems with better performance, durability and energetic efficiency. It has to be considered that, as the scale of the surfaces in contact reduces, the nature of the processes involved in the friction phenomena change dramatically. With this in mind, it is worth to remark that the development of micro and nanofabrication techniques and the use of MEMS and NEMS (Micro- and NanoElectroMechanical Systems respectively) as real alternatives in miniaturization industry, demands a new generation of specially tailored lubricants down to the molecular scale [26]. Concerning the role of friction in biological systems, phospholipid layers are strong lubricants and appear to be crucial in joint lubrication and in the composition of synovial fluid [27]. Besides, natural lubricants based on hyaluronic acid and phospholipids are essential for a reduced friction in human cartilage. For all this, several papers concerning friction at the atomic scale [28] and the molecular basis of lubrication [29] have been published recently.

Some specific applications of FFM are the study of self-assembled monolayers (SAMs) [30-37], Langmuir-Blodgett films (LBs) [38-52] and supported planar bilayers (SPBs) [16, 17]. LBs and SPBs of lipids and phospholipids are useful systems to study the behaviour of biological and biomimetic membranes [16-19, 38, 41, 52].

2.2.1 Fundamentals of FFM

The classical friction laws point out the proportionality between friction (F_F or F_L) and applied vertical force (F_V or F_N), $F_F=\mu F_V$, where μ is the friction coefficient, and the independence of F_F respect to the macroscopic contact area. These relationships are also known as the Amontons' laws. A third law, discussed in some textbooks, proposes that kinetic friction force is independent of the sliding velocity. Although Amontons' laws correlate well with macroscopic friction, some discrepancies have been detected when performing measurements in the micro- and nanoscale, partly because of the presence of an area dependent adhesion component. A more general formula that takes into account the contact area (A) is $F_F=\mu F_V+cA$, where c is a constant coefficient. The validity of this expression has been tested performing friction experiments ranging F_V from positive values to purely adhesive regimes.

Although adhesion alone is not the only interaction that modifies friction, a correlation

between them has been observed, being adhesion relatively more important for smooth or compliant surfaces and small vertical forces. In these cases, adhesion leads to violations of Amontons' laws and the relationship between F_f and F_N is not linear, as it has been experimentally detected in solid surfaces of carbon compounds [53], in SAMs [33, 35, 37] and LB films [40]. Considering Hertzian contact mechanics model [54], F_f depends on $F_N^{2/3}$, while more complex dependences, as the ones proposed in the DMT [55] and JKR [56] models, suggest different A vs. F_f dependences according to the nature of the materials in contact, that is, their stiffness and the presence of different interactions as Van der Waals, hydrophobic/hydrophilic and electrostatic forces. Down to the nanoscale, Carpick et al. extensively reviewed this methods as well as the basis of friction and recent developments in nanotribology from an experimental point of view [13]. In this direction, several works have been devoted to validate the classic contact mechanics models and to propose intermediate solutions to explain the mechanical properties of materials with varied structures and morphologies [57]. Interestingly, when the sample roughness or the F_f are high, Amontons' laws become applicable, as in many macroscopic experiments, explaining the historical origin of these laws over 300 years ago. Concerning the third Amontons' law in the nanoscopic regime, F_f increases with the logarithm of velocity to the power 2/3. Nevertheless, F_f has been observed to remain constant on carbon surfaces at velocities higher than 1 μm/s; this fact has to be studied in detail as environmental humidity, a key factor in the characterization of the two sliding interfaces, can overrule the velocity dependence of friction; condensed water necks increase the adhesion due to capillary forces, fact that inverts the velocity dependence of friction. At higher tip velocities there is less time for the condensation of water necks and there is lower friction. Consequently, the hydrophilicity of the surface plays an important role in the dependence of friction results in air conditions [11, 58].

2.2.2 The friction force technique

As the radius of the AFM tip apex is typically in the tens of nanometers range, FFM measurements gather nanotribological information, also concerning quantitative adhesion force between tip and sample, which has proved to be extremely valuable to understand the atomic and molecular origins of friction. The friction between an AFM tip and a flat solid surface has also been studied with high lateral resolution, allowing testing models that concern the atomic lattices of the surfaces [11, 13, 59].

The force sensor in FFM is either a silicon or a silicon-nitride microfabricated cantilever with a sharp tip at its end, as in AFM. The tip is brought into repulsive contact with the sample surface and the F_N applied on the tip-sample contact is measured as normal bending of the cantilever, which can be controlled by the running software of the FFM. When the sample starts sliding with respect to the tip, the lateral force acting on the tip can be recorded as a twisting of the cantilever. Figure 1 shows a scheme of the operating bases of the FFM.

In order to perform the measurements, the tip scans the sample in a direction perpendicular to the cantilever long axis (Fig. 1a) and frictional forces arise, bending the cantilever laterally. This lateral bending, which is proportional to F_f, is detected by the photodetector (a four quadrant photodetector is needed: the difference in light intensity between the two upper and lower quadrants is used to determine the vertical deflection of the cantilever, while the difference in light intensity between the left and right quadrants stands for the cantilever lateral deflection). To obtain the friction signal a friction loop has to be acquired, which means scanning a line from right to left and then from left to right (Fig. 1b). The total friction energy dissipated during these scanning processes is the area of the loop (Fig. 2) and the average F_f in the scanned line is

$$F_f = |F_{f\,(\text{left-right})} - F_{f\,(\text{right-left})}| / 2 \qquad (2)$$

To obtain quantitative results, it has to be considered that the friction signal as obtained from the microscope is in lateral photodetector volts, so the proportionality factor to obtain the

friction force has to be found. Besides, and because F_L depends on F_V, another proportionality factor has to be calculated to convert the vertical photodetector signal (V) into F_V.

2.2.3 Vertical calibration and how to calculate the applied vertical force (F_V)

AFM cantilevers are considered to behave as springs, so they have got a vertical (k_l) and lateral (k_l) force constant. This assumption is valid for moderate cantilever deflections, although deviations from ideality can occur at very high deformations. Nevertheless, the approximation is suitable if we consider that the deflection has to be followed by a laser that reflects in a photodetector and that this photodetector has a finite range of operation. In fact, the most common source of error is the non-linearity of the photodetector when the laser is far from the centre, so it is useful to check the linearity of the photodetector prior to begin the friction experiments (Fig. 3).

Several methods have been implemented to find the vertical force constant k_l of AFM cantilevers. Sader et al. proposed a method that has into account the geometry of the cantilever and its density [60]. Nevertheless, as cantilevers are structures usually conformed by layers of several materials (usually a chromium and a gold layer is deposited on the cantilever back to improve laser reflection, conductive cantilevers can have different metallic coatings, etc.), the error in the density calculus can be high. Besides, the thickness of the cantilever has to be experimentally measured. Further improved models use the cantilever resonant frequency and its Q factor as parameters, so density and cantilever thickness measurements are not necessary [61]. Unfortunately, these calculations are valid for beam shaped cantilevers and to apply them to triangular cantilevers it is necessary to have a chip with triangular and beam shaped cantilevers together and assume that the thickness of all of them is constant.

Cleveland et al. proposed to measure the resonant frequency shift as a mass is added to the cantilever to calculate the vertical spring constant [62]. Practically, tungsten microspheres are deposited on a glass slide and picked up by the cantilever by capillarity forces. The distance between the free end of the cantilever and the microsphere has to be accurately measured because it strongly influences the resonance frequency shift. The most important handicap of this method is that it is difficult to calculate the mass of the attached microsphere because of the indetermination in the material density and the deviation from the spherical shape.

Thermal noise method uses the small oscillation of the cantilever due to thermal energy to calculate its vertical force constant [63]. This model is valid for beam shaped and triangular tips, although it is not suitable for stiff cantilevers because the amplitude of the resonance is too small to be detected. Between its drawbacks we can find that the obtained force constant varies significatively depending on the laser position on the cantilever and on the medium where the measurements are performed (air, water or vacuum).

If a reference cantilever with a known force constant is available, other cantilevers can be vertically calibrated. The technique consists on pushing the reference cantilever with the uncalibrated one. Measuring the deflection while knowing the vertical piezo movement, gives an accurate measurement of the vertical force constant [64]. A recent work has been devoted to compare and validate some of these vertical calibration methods [65].

In order to convert the vertical photodetector signal into F_V, vertical sensitivity (S_V), which is the relationship between the cantilever deflection and the variation of vertical photodetector signal, is needed. Then,

$$F_V = k_V \cdot S_V \cdot C_D \tag{3}$$

where C_D is the vertical cantilever deflection. When the tip and the sample are in contact and a force curve is performed, we can consider that

$$Z_{PD} = S_P + C_D \tag{4}$$

being Z_{PD} the Z piezo displacement and S_P, the sample penetration (Fig. 4). Now, if a force curve is performed on an undeformable material (SiO_2, diamond, etc.):

$$Z_{PD} = C_D \text{ (as } S_P \sim 0) \qquad (5)$$

In this case, the slope of the force curve is $1/S_V$. S_V varies from tip to tip, but it also can change noticeably after repositioning the laser due to cantilever buckling.

2.2.4 Lateral calibration and how to calculate the friction force (F_F)

Several methods have been proposed in the past to find k_L and lateral sensitivity (S_L). Green et al. extended Sader's geometrical method to find k_V also to find k_L, as well as Cleveland did for its added mass method [66]. Liu et al. [67] proposed a method concerning the calibration of the lateral response of the photodetector as a function of the torsion angle of the cantilever while performing the friction measurements and Cain et al. [68] analyzed the static friction arisen between tip and sample in order to infer the mechanical constants of the cantilevers. Although studies comparing these methods demonstrate that they are consistent and render quantitative values [69], perhaps the method proposed by Ogletree et al. [70] is the most widely used. It is based on the fact that friction is dependent on the slope of the sample. Then, if a sample with well known slopes is scanned at variable F_V while recording the friction signal, k_L and S_L can be calculated. $SrTiO_3$, after being conveniently annealed, shows (001) and (100) crystalline faces forming sharp ridges, so it can be used to laterally calibrate the tips. Nowadays, sample calibration grids with sharp edges are also available in the market for this purpose. It is important to note that the calibration obtained by this technique is dependent on the position of the laser and also on the position of the photodetector. In the vast majority of commercial AFM systems, the photodetector physical movement is coupled between the X and the Y axis, so when it moves in one axis, the laser spot also moves in the other. This effect can be due to a misalignment of the laser path respect to the photodetector or because of a mechanical coupling of the screws that move it. In all cases, moving the photodetector changes S_L and, consequently, the validity of the calibration. This effect can be a major problem when compliant tips are used (0.01-0.1 N/m) because the laser position on the photodetector can derive importantly with time and also with humidity.

3. STUDY OF SUPPORTED LIPID BILAYERS AND LANGMUIR-BLODGETT FILMS

3.1 FFM/AFM/FS of Supported Lipid Bilayers

In order to study the properties of biological membranes, the use of liposomes deposited on solid supports has become very usual [71-74]. Supported lipid bilayers, SLB's, which are formed by deposition of lipid vesicles or liposomes on solid supports as mica, glass or silica [75], can also incorporate proteins, fact that provides access to basic aspects of membrane biophysics and membrane-protein interactions [2, 3].

The friction behaviour of DMPC in SPB deposited on mica was investigated in liquid environment by LFM and the effect of sodium chloride (NaCl) was tested at several concentrations, ranging from 0 to 0.1 M [17]. Some theoretical calculations have revealed the critical role of NaCl in the structure of phospholipid bilayers and shown that the phospholipid polar heads pack in a more compact way in the presence of NaCl [76, 77]. This has been experimentally confirmed from force spectroscopy measurements on several SPBs of DMPC, DLPC, DPPC and POPE [78, 79].

The DMPC bilayers were deposited on mica from aqueous solutions containing a certain NaCl concentration and buffered at pH 7.0 with TRIS. After deposition, samples where washed with saline solutions of the same NaCl concentration and finally the same saline solution was poured onto the sample in order to perform the AFM and FFM experiments in liquid environment (for more details see [17]).

The obtained DMPC bilayers show a height of ca. 6 nm. Bilayers break under the pressure exerted by the tip, giving a typical discontinuity in the indentation curve (breakthrough) (see Fig. 3 in [17]). Interestingly, breakthrough force depends on the NaCl concentration, that is, force increases when NaCl concentration increases, highlighting the effect of ions in the mechanical properties of the bilayer. In a similar way, friction experiments also reveal the influence of the NaCl concentration. Figure 5 shows F_f vs. F_V for each NaCl concentration. Three friction regimes can be observed as F_V increases. The initial region presents a near null friction coefficient, which is the slope of the F_f vs. F_t curve. This initial region ends when F_t is high enough to create defects on the surface of the bilayer, process that is marked with a F_f increase. The F_V at which the bilayer breaks increases with the NaCl concentration. At higher F_V, a third region can be observed, where the friction coefficient tends to the friction coefficient of mica, fact that is attributed to the contact between the tip and the mica substrate. Concerning the kinetics of the friction process, topographic images show that the broken bilayers recover more easily when the NaCl concentration is low. These facts point to a higher compactness and stiffness of the bilayers as ionic strength increases.

The friction behaviour and the indentation curves can be related to the phospholipid bilayer structure and, in particular, to the influence of electrolyte ions. At low F_V (first region) the tip and the bilayer experiment a repulsive electrostatic interaction. This effect is predicted and quantified by the Derjaguin-Landau-Verwey-Overbeek (DLVO) theory for two surfaces negatively charged. Silicon nitride tips at these experimental conditions have negative charge and it has also been reported that the negative charge of DMPC bilayer also increases with NaCl concentration. This repulsive electrostatic interaction explains the low friction observed in this first region, which broadens when increasing NaCl concentration. In addition, the screening effect of the ions in solution over the charges present in DMPC polar heads explains the higher compactness and stiffness of the bilayer when increasing the ionic strength; Na^+ ions penetrate the DMPC polar heads with a Na^+/DMPC ratio that increases with NaCl concentration. The presence of positive ions in the polar heads reduces the electrostatic repulsion between negative phosphates, while the repulsion between positive choline groups is reduced by Cl^- ions, which have also been predicted to interact with the polar heads. Besides, Cl^- ions are partly responsible for the negative charge of the DMPC bilayers detected by the tip (see Fig. 7 in [17]). At higher F_V, the tip punctures the layer and then is capable of disorganize it and eventually create a "permanent" hole during the scan, especially when the cohesion between the layer molecules is higher. This occurs at higher NaCl concentrations, when the layer presents higher stiffness and is unable to restructure after the tip scan. On the contrary, at lower NaCl concentrations the cohesion between molecules in the bilayer is lower, the bilayer is less rigid and it recovers more easily after the tip scan. The influence of NaCl in the mechanical properties of phospholipid bilayers has been also discussed by Pandit et al. [80] and by Böckmann and Grubmüller [76].

The effect of the electrolyte ions on DMPC has also been studied by measuring the zeta potential value of the SPB in solution varying the pH and the ionic strength. On one hand, the zeta potential decreases (becomes more negative) as pH increases while keeping constant the ionic strength and the topographic AFM images show the clear influence of the pH (see Fig. 1 in [79]). As pH increases and zeta potential consequently decreases, the SPB shows more defects than at low pH values, where the obtained bilayer is continuous. On the other hand, the zeta potential increases with the ionic strength while keeping constant the pH, and the AFM images show a more compact bilayer at higher ionic strengths (see Fig. 3 in [79]). Then, for both pH and ionic strength variations, it is observed that high compacity bilayers are obtained when zeta potential is positive. These observations are not influenced by the supporting material being hydrophilic, negatively charged mica or silicon oxide.

Another aspect is the kinetics of the incorporation of ions into the phospholipid

polar head group. Experiments in our group [78] proved that this is a fully reversible process with relatively fast kinetics in the timescale of the experiment (10-15 min), which makes it measurable with force spectroscopy.

When PC phospholipids others than DMPC (C14:0) are investigated, as DLPC (C12:0), DPPC C16:0) and DOPC (C18:1), similar general trends have been observed, but now it is possible to discuss the influence of the chain length and the number of unsaturations. Breakthrough force increases with the chain length when ions are present in solution, but a weaker influence when pure water is used was detected (see Fig. 12 in [78]). Then, the longer the tail, the higher the attractive interactions and the compactness, which are also favoured by the presence of ions. On the other hand, the presence of an unsaturation, tested experimentally using DOPC, reduces the breakthrough force, due to a decrease in layer compactness.

The overall tendencies discussed before in mimetic SLB have been also observed in a natural lipid bilayer (Escherichia coli lipid extract) [78]. In conclusion, it is worthwhile to highlight that monovalent cations, e.g. Na^+, play an important role in the mechanical properties and stability of bilayers and membranes, so far underestimated. The ions bound into the membrane promote the increase in lateral interactions (higher phospholipid-phospholipid interactions, decrease in area per lipid), giving rise to a more packed phospholipid network, which can be mechanically tested both with force spectroscopy or friction measurements.

The mechanical properties of DOPC bilayers have been studied by LFM and AFM force spectroscopy in a liquid environment [16]. Grant and Tiberg reported low F_F values as long as the supported layer resisted the normal pressure of the tip, but high F_F values when the F_V exceeded the critical value needed for puncturing the layer. F_L vs F_V curves follow a linear relationship, according to the phenomenological Amontons' law. These authors have also found a direct correlation between the breakthrough force and the compactness or density of the SPB. A similar correlation has been found for DOPC monolayers adsorbed on a hydrophobic surface, as well as for the friction behaviour. They also estimated the critical load for lipid layer rupture to be larger than 10 kg/cm^2 for the layers studied by them. Figure 8 in [16] shows a clear correlation between the friction and vertical force curves. This correlation has also been observed by Oncins et al. [17].

The force needed to puncture the membrane has been reported to depend also on the tip approaching velocity [81, 82], on the chemical composition of the system [10, 18] and on the thermodynamic phase of the lipid (temperature) [82, 83].

3.2 FFM/AFM of Langmuir-Blodgett films

The physicochemical and structural properties of phospholipid [84] and fatty acid monolayers and bilayers have been studied using Langmuir and Langmuir-Blodgett films which, besides natural membranes, provide good biomimetic systems. As an example, lipidic LB films have been used as substrates to intercalate proteins, which are a field that has awakened a great deal of interest in the scientific community and that has been reviewed recently [85]. Concerning the characterisation of lipidic LB films, AFM has become a powerful technique, mostly concerning topographic studies. As a complementary technique, FFM can provide new insights in the study of biomimetic LB systems, especially in respect to their chemomechanical properties, which have also been studied with AFM spectroscopy [18]. Surface properties of mixed phospholipid monolayers and bilayers have been studied by Dufrêne et al. [19]. With this combination of SPM techniques, the presence of domains in natural or mimetic membranes, or in mixed LB films of a fatty acid and a protein [38], has been observed.

The LB technique permits the control of the film surface pressure, and then provides a way to study the influence of this factor on the membrane behaviour. A friction study has been done in LB films by Oncins et al. [40] where

the influence of the subphase and the extraction pressure are shown. Interesting features in the structure of the LB films were revealed through friction, as the presence of an asymmetric response in the forward and reverse scan on island structures, and the existence of different stages in island formation with changes in the friction response. Friction anisotropy and asymmetry were previously observed by Liley et al [41] in lipid monolayers transferred onto mica, and the authors correlated these effects with the tilt direction of the alkyl chains. It was observed that even small molecular tilts can make a major contribution to friction. The organization of monoacylglycerol monolayers have also been studied by FFM [45-47].

Dufrene et al. [19] investigated phase separation in LB monolayers and bilayers of DSPE and DOPE and found a significant contrast in adhesion and friction between DSPE domains embedded in a DOPE matrix, despite the two phospholipids shared the same head group. This effect was attributed to a difference in the film mechanical properties, the DOPE phase being inelastically deformed by the probe. Later, AFM images of phase-separated mixed phospholipid SLBs performed by Schneider et al. [18] showed a high topographic contrast at loads between the breakthrough force of each phase and a low topographic contrast at loads above the breakthrough force of both phases. Interestingly, these authors have found that frictional contrast is inverted and magnified at loads above the breakthrough force of both phases. For all this, the breakthrough force is an important parameter in the characterisation of supported films.

The friction response of LB films vs. the applied normal forces (friction force spectroscopy), provides information on the friction and adhesion response and also shows the film breakthrough force. This force can also be obtained from force curves, although the involved processes are not the same because during friction experiments, the tip slides laterally on the sample, while force spectroscopy is performed on a single spot on the surface. Friction properties of LB films of fatty acids are being investigated by the authors. Some preliminary data are shown in Figure 6, where it can be seen the behaviour of LB films of arachidic acid at different deposition surface pressures. A marked increase in the F_F is observed when the breakthrough force is reached, which in turn increases with the surface pressure. These results open the way to investigate, in the near future, the influence of several factors, such as chain length, head group, pH, ionic strength, temperature and especially surface pressure, on the nanomechanical and nanotribological behaviour of LB films of fatty acids and lipids by using the friction force microscopy and spectroscopy.

ACKNOWLEDGMENT

The authors thank the financial support of the project MCYT CTQ2004-08046-C02.

GLOSSARY

AFM: atomic force microscopy

DMPC: 1,2-dimyristoyl-sn-glycero-3-phosphocholine

DOPC: 1,2-dioleoyl-sn-glycero-3-phosphocholine

DLPC: 1,2-dilauroyl-sn-glycero-3-phosphocholine

DPPC: 1,2-dipalmitoyl-sn-glycero-phosphocholine

DLVO: Derjaguin-Landau-Verwey-Overbeek

DMT: Derjaguin, Muller and Toporov

FFM: friction force microscopy (=LFM)

JKR: Johnson, Kendall and Roberts

LB: Langmuir-Blodgett

LFM: Lateral Force Microscopy (=FFM)

POPE: 1-palmitoyl-2-oleoyl-sn-glycero-3-phosphocholine

SPB: supported planar bilayers

SLB: supported lipid bilayers

SPM: scanning probe microscopy

TRIS: 1,1,1-triphenil-3,3,3-tris(m-tolyl)-disiloxane

REFERENCES

1. Ceve, G., 1990, Biochim. Biophys. Acta, 1031, 311.
2. Mueller, H., Butt, H.J., and Bamberg, E., 2000, J. Phys. Chem. B, 104, 4552.
3. Desmeules, P., Grandbois, M., Bondarenko, V.A., Yamazaki, A., and Salesse, C., 2002, Biophys. J. 82, 3343.
4. Vliet, K.J. van, and Hinterdofer, P., 2006, Nanotoday, 1(3), 18.
5. Dufrêne, Y.F., 2003, Current Opinion in Microbiology, 6, 317.
6. Charras, G., Lehenkari, P., and Horton, M., 2002, Biotechnological Applications of AFM, Chap 8 in Methods in Cell Biology, vol 68, Jena, B.P., and Hörber, H.J.K. (Eds.), Academic Press.
7. Pera, I., Stark, R., Kappl, M., Butt, H-J., and Benfenati, F., 2004, Biophys. J., 87, 2446.
8. Ebenstein, D.M., and Pruitt, L.A., 2006, Nanotoday, 1(3), 26.
9. Sanz, F., Fraxedas, J., Gorostiza, P., and Garcia-Manyes, S., 2002, Contributions to Science, 2(2), 173.
10. Dufrene, Y.F., Boland, T., Schneider, J.W., Barger, W.R., and Lee, G.U., 1998, Faraday Discuss., 111, 79.
11. Bennewitz, R., 2005, Materials Today, 8(5), 42.
12. Gnecco, E., Bennewitz, R., Gyalog, T., and Meyer, E., 2001, J. Phys.: Condens. Matter, 13, R619.
13. Carpick, R.W., and Salmeron, M., 1997, Chem. Rev., 97, 1163.
14. Dufrêne, Y.F., and Lee, G.U., 2000, Biochimica et Biophysica Acta, 1509, 14.
15. Takano, H., Kenseth, J.R., Wong, S-S., O'Brien, J.C., and Porter, M.D., 1999, Chem. Rev. 99, 2845.
16. Grant, L.M., and Tiberg, F., 2002, Biophys. J., 82, 1373.
17. Oncins, G., Garcia-Manyes, S., Sanz, F., 2005, Lang., 21, 7373.
18. Schneider, J., Dufrêne, Y.F., Barger Jr.,W.R., and Lee, G.U., 2000, Biophys. J., 79, 1107.
19. Dufrêne, Y.F., Barger, W.R., Green, J-B.D., and Lee, G.U., 1997, Lang., 13, 4779.
20. Byfield, F.J., Aranda-Espinoza, H., Romanenko, V.G., Rothblat, G.H., and Levitan, I., 2004, Biophys. J., 87, 3336.
21. Méléard, P., Gerbeaud, C., Bardusco, P., Jeandaine, N., Mitov, M.D., and Fernandez-Puente, L., 1998, Biochim., 80, 401.
22. Olbrich, K., Rawicz, W., Needham, D., and Evans, E., 2000. Biophys. J., 79, 321.
23. Lee, C-H., Lin, W-C., and Wang, J., 2001, Phys. Rev. E, 64, 020901(R).
24. Binnig, G., Rohrer, H., Gerber, Ch., and Weibel, E., 1982, Applied Physics Letters, 40, 178.
25. Binnig, G., Quate, C. F., and Gerber, C., 1986, Phys. Rev. Lett., 56, 930.
26. Flater, E.E., Corwin, A.D., de Boer, M.P., and Carpick, R.W., 2006, Wear, 260, 580.
27. Schwarz, I.M., and Hills, B.A., 1998, J. Rheumatol., 37, 21.
28. Ringlein, J., and Robbins, M.O., 2004, Am. J. Phys., 72, 884.
29. Hsu, S.M., 2004, Tribol. Int., 37, 553.
30. Leggett, G.J., 2003, Anal. Chim. Acta, 479, 17.
31. Chen, J., Ratera, I., Murphy, A., Ogletree, D.F., Fréchet, J.M.J., and Salmeron, M., 2006, Surf. Sci., 600(18), 4008.
32. Carpick, R.W., Sasaki, D.Y., and Burns, A.R., 1999, Tribol. Lett., 7, 79.
33. Xiao, X., Hu, J., Charych, D.H., and Salmeron, M., 1996, Lang., 12, 235.
34. McDermott, M.T., Green, J-B.D., and Porter, M.D., 1997, Lang., 13, 2504.
35. Lio, A., Charych, D.H., and Salmeron, M., 1997, J. Phys. Chem. B, 101, 3800.
36. Fujihara, M., Tani, Y., Furugori, M., Akiba, U., and Okabe, Y., 2001, Ultramicroscopy, 86, 63.
37. Brukman, M.J., Oncins, G., Dunbar, T.D., Boardman, L.D., and Carpick, R.W., 2006, Lang., 22, 3988.
38. Sommer, F., Alexandre, S., Dubreuil, N., Lair, D., Duc, T-m., and Valleton, J.M., 1997, Lang., 13, 791.
39. Oishi, Y., Umeda, T., Kuramori, M., and Suehiro, K., 2002, Lang., 18, 945.
40. Oncins, G., Torrent-Burgues, J., and Sanz, J., 2006, Tribol. Lett., 21, 175.

41. Liley, M., Gourdon, D., Stamou, D., Meseth, U., Fischer, T.M., Lautz, C., Stahlberg, H., Vogel, H., Burnham, N.A., and Duschi, C., 1998, Science, 280, 273.
42. Meyer, E., Overney, R., Lüthi, R., Brodbeck, D., Howald, L., Frommer, J., Güntherodt, H-J., Wolter, O., Fujihira, M., Takano, H., and Gotoh, Y., 1992, Thin Solid Films, 220, 132.
43. Xue, Q.J., and Zhang, J.. 1995, Tribol. Int., 28, 287.
44. Yokoyama, S., Kakimoto, M., and Imai, Y., 1996, Synthetic Metals, 81, 265.
45. Gehlert, U. Fang, J., and Knobler, C.M., 1998, J. Phys. Chem B, 102, 2614.
46. Meine, K., Vollhardt, D., and Weidemann, G., 1998, Lang., 14, 1815.
47. Hisada, K., and Knobler, C.M., 2000, Lang., 16, 9390.
48. Zhang, P., Lu, J., Xue, Q., and Liu, W., 2001, Lang., 17, 2143.
49. Matsumoto. M., Tanaka, K-i., Azumi, R., Kondo, Y., and Yoshino, N., 2003, Lang., 19, 2802.
50. Zhang, P., Xue,Q., Du, Z., and Zhang, Z., 2003, Wear. 254, 959.
51. Xu, S-L., Kang, S-Z., Deng, G-J., Wu, P.. Fan, Q-H., Wang, C., Wan, L-J., and Bai, C-L., 2003, Chem. Lett., 32, 290.
52. Ekelund, K., Sparr, E., Engblom, J., Wennerström, H., and Engström, S., 1999, Lang., 15, 6946.
53. Schwarz, U.D., Zwörner, O., Köster, P., and Weisendanger, R., 1997, Phys. Rev. B, 56(11), 6987.
54. Hertz, H.. and Reine, J., 1882, Angew. Mathematik, 92, 156.
55. Derjaguin, B. V., Muller, V. M., and Toporov, Y. P., 1975, J. Colloid Interface Sci., 53, 314.
56. Johnson, K. L., Kendall, K., and Roberts, A. D., 1971, Proc. R. Soc. London A, 324, 301.
57. Carpick, R.W., Ogletree, D.F., and Salmeron, M., 1999, J. Colloid Interf. Sci., 211, 395.
58. Riedo, E., Lévy, F., and Brune, H., 2002, Phys. Rev. Lett., 88(18), 185505.
59. Carpick, R.W., Dai, Q, Ogletree, D.F., and Salmeron, M., 1998, Trib. Lett., 5(1), 91.
60. Sader, J.E., 1995, Review of Scientific Instruments, 66(9), 4583.
61. Sader, J.E., Chon, J.W., and Mulvaney, P., 1999, Review of Scientific Instruments, 70(10), 3967.
62. Cleveland, J. P., Manne, S., Bocek, D., and Hansma, P. K., 1993, Review of Scientific Instruments 64, 403.
63. Hutter, J.L., and Bechhoefer, J., 1993, Review of Scientific Instruments, 64(7), 1868.
64. Torii, A., Sasaki, M., Hane, K., and Okuma, S., 1996, Measurement Science and Technology, 7, 179.
65. Lévy, R., and Maaloum, M., 2002, Nanotechnology. 13, 33.
66. Green, C.P., Lioe, H., Cleveland, J.P., Mulvaney, P., and Sader, J.E., 2004, Review of Scientific Instruments, 75(6), 403.
67. Liu, E., Blanpain, B., and Celis, J.P., 1996, Wear, 192, 141.
68. Cain, R.G., Page, N.W., and Biggs, S., 2000, Journal of Colloid and Interface Science, 227, 55.
69. Cain, R.G., Reitsma, M.G., Biggs, S., and Page, N.W., 2001, Review of Scientific Instruments, 72(8), 3304.
70. Ogletree, D.F., Carpick, R.W., and Salmeron, M., Review of Scientific Instruments, 67, 3298.
71. McConnell, H.M., Watts, T.H., Weis, R.M., and Brain, A.A., 1986, Biochim. Biophys. Acta, 864, 95.
72. Richter, R.P., Him, J.L.K., and Brisson, A., 2003, Mater. Today, 6(11), 32.
73. Sackmann, E., 1996, Science, 271, 43.
74. Castellana, E.T., and Cremer, P.S., 2006, Surf. Sci. Reports, 61(10), 429.
75. Richter, R.P., Bérat, R. and Brisson, A.R., 2006, Langmuir, 22, 3497.
76. Böckmann, R., and Grubmüller, H., 2004, Angew. Chem. Int. Ed., 43, 1021.
77. Böckmann, R., Hac, A., Heimburg, T., and Grubmüller, H., 2003, Biophys. J. 85, 1647.
78. Garcia-Manyes, S., Oncins, G., and Sanz, F., 2005, Biophys. J., 89, 1812.
79. Garcia-Manyes, S., Oncins, G., and Sanz, F., 2006, Electrochim. Acta, 51, 5029.
80. Pandit, S.A., Bostick, D., and Berkowitz, M.L., 2003, Biophys. J., 84, 3743.
81. Loi, S., Sun, G., Franz, V., Butt, H.J., 2002, Phys. Rev. E, 66, 031602.
82. Franz, V., Loi, S., Muller, H., Bamberg, E., and Butt, H.H., 2002, Colloids Surf. B, 23, 191.
83. Garcia-Manyes, S., Oncins, G., and Sanz, F., 2005, Biophys. J., 89, 4261.
84. Domènech, O., Torrent-Burgués, J., Merino, S., Sanz, F., Montero, M.T., Hernández-Borrell, J., 2005, Colloids Surf. B, 41, 233.

85. Girard-Egrot, A.P., Godoy, S., and Blum, L.J., 2005, Adv. Colloid Inter. Sci., 116, 205.

FIGURES

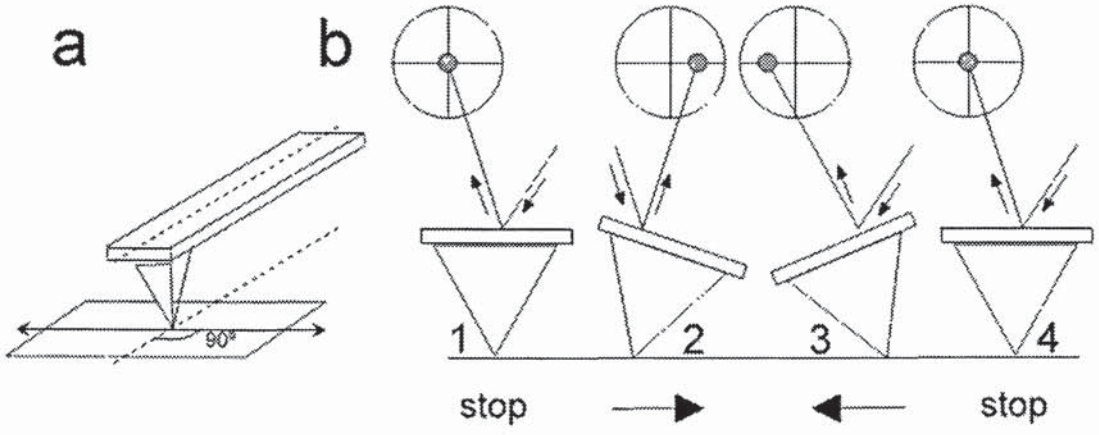

Figure 1. Scheme of the operating bases of the Friction Force Microscope. a) Direction of scanning when performing friction measurements. The scanning has to be perpendicular to the main cantilever axis to enable the cantilever torsion during sliding. b) Front tip view while performing a friction loop. 1. The tip lays still on the surface. 2. The probe scans to the right and the cantilever lateral deflection is recorded in the photodetector. 3. The probe scans to the right and the signal in the photodetector changes. 4. Scanning stops.

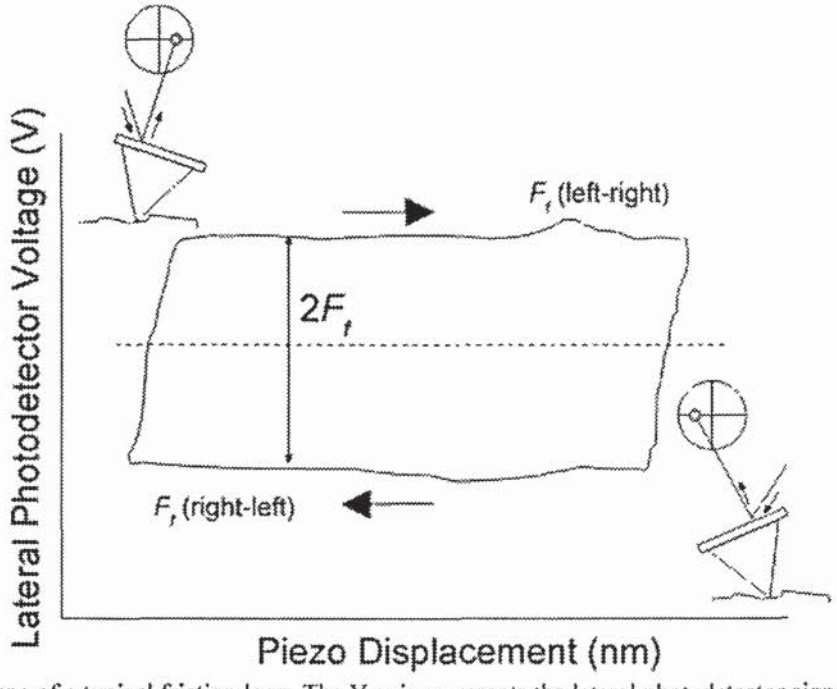

Figure 2. Shape of a typical friction loop. The Y axis represents the lateral photodetector signal as the tip slides on the sample surface. The Y axis can be converted to F_f if the lateral force constant (k_l) and the lateral sensitivity (S_L) of the cantilever are known.

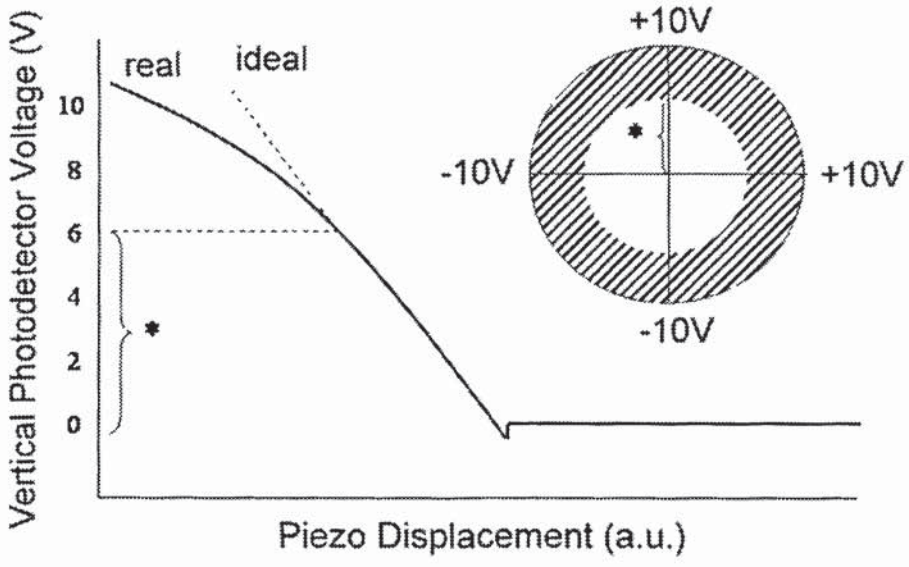

Figure 3. Photodetector response. Force curves can be used to check both the linearity of the photodetector and the assumption that the cantilever behaves as an ideal spring. This imaginary photodetector with a range of ±10V in vertical and lateral axis is linear in the region ±6V if radial symmetry is assumed (non-linear region is stripped in the photodetector cartoon and the linear region in the vertical positive axis is marked with a * both in the force curve and in the photodetector). As a result, no quantitative measurements can be obtained in the stripped region.

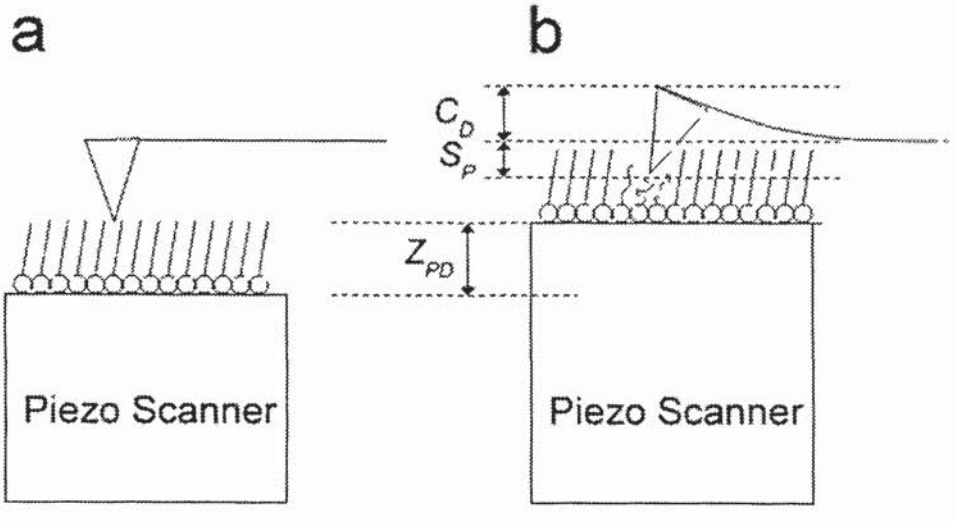

Figure 4. Sample and cantilever deformation as a force curve is performed. a) The tip and the sample are in contact, prior to any cantilever deflection or sample deformation. b) As the Z piezo moves the sample up (Z_{PD}), the cantilever deflects (C_D) and the sample is penetrated (S_P) according to $Z_{PD} = S_P + C_D$

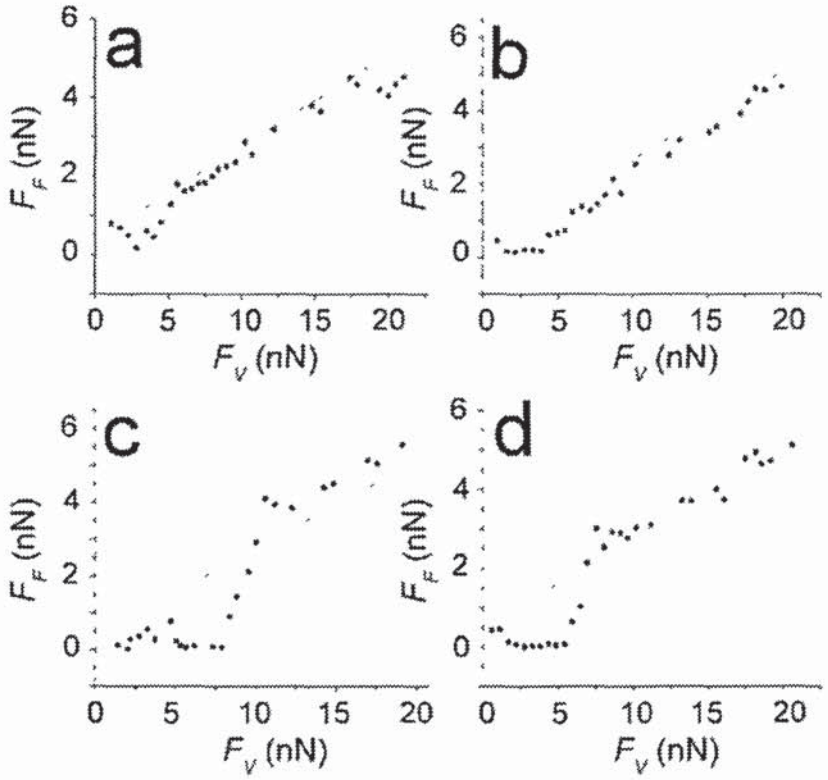

Figure 5. F_f vs. F_t curves on DMPC bilayers in an aqueous environment. NaCl concentration is (a) 0 M, (b) 0.01 M, (c) 0.05 M, and (d) 0.1 M. The error bars represent the confidence intervals (at 95%, number of samples 256). A reference F_f vs. F_t curve obtained on mica is included in every panel (dashed line).

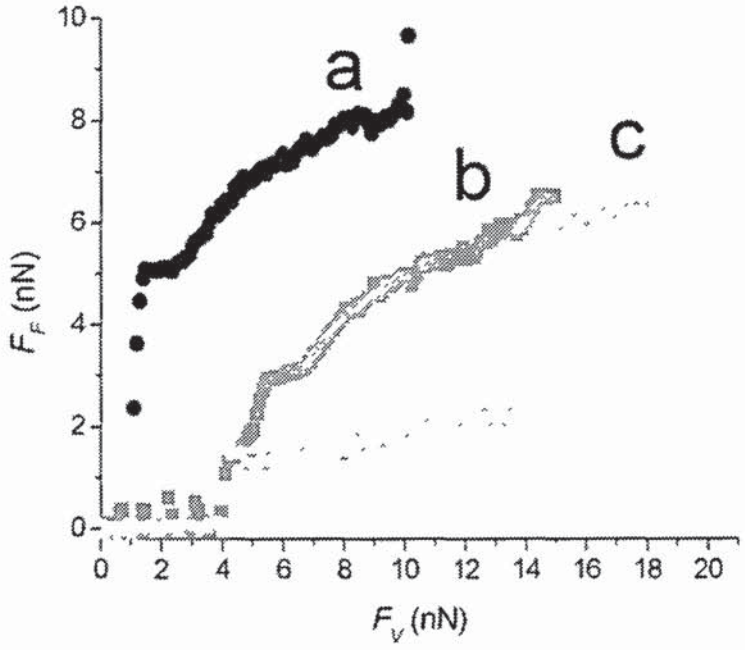

Figure 6. F_f vs. F_t curves performed on arachidic acid LB films. The extraction pressure is: a) 1mN/m, b) 15mN/m, c) 35mN/m.

Chapter 4

4.Engineering coatings for MEMS and NEMS. A step towards future

4.1 INTRODUCTION

In our everyday live, we use and interact with a wide variety of mechanical and electrical devices, from the toaster that prepares our breakfast to the bus that takes us to work. What had seemed a fairytale for our grandparents now is a quotidian reality that we take for granted. The step further came with the development of microelectronics and the astounding computer boom. It is quite difficult to keep pace with the latest released microprocessor or the all-in-one gadgets that, being not bigger than a cigarette box, let you connect with the rest of the world. In this blossoming field that has become the microelectronics industry, accessory systems and mobile pieces must be miniaturized more and more in order to provide reliable and durable devices ready for being used and abused. Once again, science comes to solve everyday live problems.

4.2 WHAT ARE MEMS AND NEMS?

Micro Electro Mechanical Systems (MEMS)[116-118] and Nano Electro Mechanical Systems (NEMS)[119,120] are devices that are able to create a mechanical movement thanks to the application of an electrical field or vice versa. In other words: machines. The unique thing about these systems is their size; while the

MEMS are in the range that goes from 1 mm to hundreds of micrometers, the NEMS go still further (or closer), comprehending all the devices that have components that are smaller than 100 nm. These systems can be used by their mechanical or electrical functionality but also because of their optical or biological functions, in the so-called BioMEMS[121-123] and BioNEMS[124].

4.2.1 Facing the truth: the volume/surface issue

As devices become smaller, the volume/surface ratio changes, so the forces that affect macroscopic machines will not affect our MEMS and NEMS the same way. To give an example, if the dimensions decrease from 1 mm to 1 μm, the area decreases 1 million times, while the volume decreases 1000 million times (you can find a more graphic example of the same effect in fig. 19). As a consequence, it is clear that the forces that are surface-related will determine the way the micro- and nano-devices behave. Then, adhesion, friction and liquid meniscus forces, which are interactions that are proportional to the area) will be more relevant than electromagnetic or inertial forces (proportional to volume)[125]. Another fact that must be taken into account is that, as pieces decrease in size, the fabrication tolerances also decrease and contact phenomena between different parts become more likely, increasing the presence of adhesive and frictional effects[121]. In addition, spurious contamination, which is not that small when it comes to MEMS and specially NEMS, can pose serious wearing problems[126]. If the whole picture did not look frightening enough, we must consider the condensation of water on mobile parts and contacts; its presence increases the static friction a lot, posing a really serious problem to the reliability and robustness of MEMS and NEMS[127,128]. In this sense, the pioneer experiments performed in Sandia show how a micro-gear gets stuck after completing a few cycles[129] (Fig. 20).

Let's see how some prototypes and commercial designs work and which are the specific surface problems that arise when it comes to have such small devices

running. Some solutions to stiction and wear problems will also be pointed out, although they will be treated in more detail in the next section.

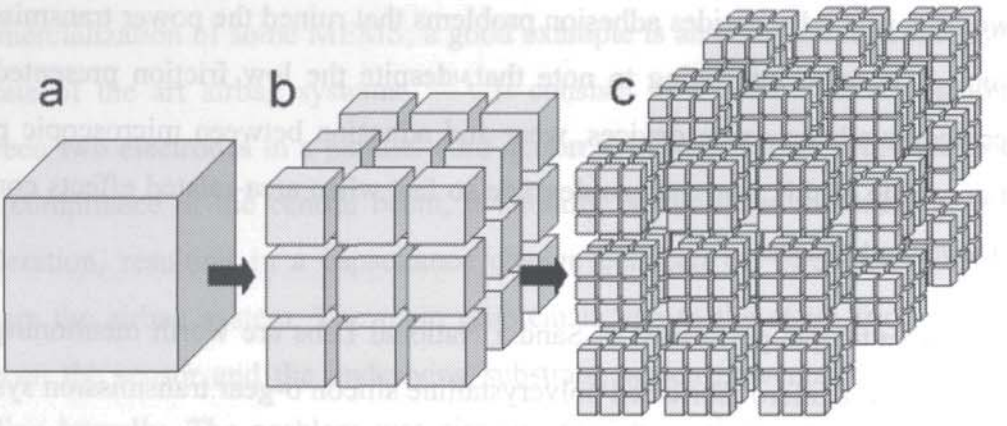

Fig. 19. The surface issue in small bodies. While a), b) and c) have the same volume, the surface of a) is multiplied by 9 in b), while it is multiplied by 54 in c). As you may suspect, the surface phenomena that probably have a negligible effect on the mechanical behavior of a), become dominant in c). Now imagine how many times you have to divide the dimensions of a macroscopic machine to get into the NEMS range and you will take a glimpse of the difficulties MEMS and NEMS manufacturers have to deal with!

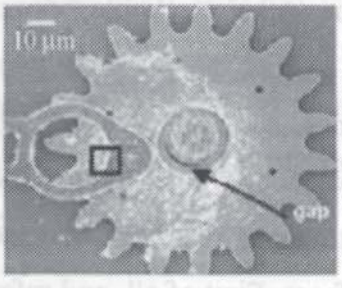

Fig. 20. Micrometric gear showing serious wear problems. Courtesy of Sandia National Laboratories, SUMMiTTM Technologies, webpage; www.mems.sandia.gov.

4.3 MEMS

Tai et al. reported an electrostatic motor based on a 12 stator and a 4-pole rotor design produced by micromachining techniques[130]. The diameter of the rotor was 120 µm and the gap between the rotor and the stators was just 2 µm. Although the motor was able to spin at 100000 rpm, the intermittent contact between the rotor and stators resulted in serious wear problems, which compromised the reliability of the device. A posterior attempt[131] consisted in fabricating a bladed

stator-rotor pair entirely in silicon with sub micrometric dimensions to be used in a micro-gas turbine at 1000000 rpm, but blades erosion prevented the whole system of working properly, besides adhesion problems that ruined the power transmission system. It is quite interesting to note that, despite the low friction presented by macroscopic silicon oxide devices, wear and adhesion between microscopic parts that are made of this material can degrade so fast when area-related effects control the movement process.

The attempts performed in Sandia National Labs are worth mentioning, as they produced a micro fabricated polycrystalline silicon 6-gear transmission system and also a micro gear speed reduction system that was tested in air conditions[132]. Unfortunately, the performance of the systems was not good because of gear teeth breakage due to lateral stresses. Wear due to humidity condensation was also reported. The silicon parts were coated with tungsten in an attempt to reduce adhesion, friction and meniscus interactions. Although the mechanical behavior of the systems improved it was still not reliable because of the poor tungsten film yield. A novel strategy was to coat the gears with vapor deposited self assembled monolayers (SAMs) of silanes. Although the coating quality was satisfactory, the monolayer removed from contacting parts after a few cycles due to wear. In this specific case, we see two strategies that have become common in order to reduce friction between sliding surfaces. First of all, and referring to the tungsten case, the application of hard coatings that increase the mechanical durability of the parts in mechanical contact. In fact, this is a well-known strategy in the macroscopic world and represents the difference between a 1$ and a 50$ screwdriver. Respect to the coating with organic monolayers, the similarity with our macroscopic sense of reality is not so straightforward, as monolayers are a truly molecular surface science concept. Nevertheless, the analogy would be the lubricants that are used in car engines and that prevent metallic parts of contacting each other and triggering grinding processes. As the dimensions grow smaller, liquid lubricants make no sense and the development of suitable organic monolayers with low friction and high adherence to the substrate are the nanotribology Holy Grail.

4.3.1 MEMS in the market

The development of micro fabrication techniques has led to the commercialization of some MEMS; a good example is an accelerometer integrated in state of the art airbag systems[133,134]. It consists in a beam that is positioned between two electrodes in a parallel conFig.tion as shown in Fig. 21*a*. Due to the high compliance of the central beam, it laterally bends under the exertion of an acceleration, resulting in a capacitance change between the two electrodes that triggers the airbag system. The main problem is due to the static friction arisen between the sensor and the underlying substrate, which prevents the beam from bending laterally. The problem was circumvented by covering the whole system with a silane solution. As the sensor is sealed and heated in a furnace, the solvent evaporates and the beams are covered by a silane monolayer that highly reduces static friction and improves the performance of the device. Another interesting application are pressure sensing MEMS, which are used for tires and blood pressure monitoring devices[135] (Fig. 21*b*). They are based on a pressure sensitive membrane, the movement of which is monitored by a set of piezoresistors. As the whole system is subjected to extreme changes in temperature and also to hostile chemical environments, it usually fails because of corrosive and erosive wear or because of membrane fracture.

Finally, I would like to mention a MEMS that takes advantage of the predominance of surface forces at the micro-scale. The name of the device is Nanotractor® and was developed in Sandia by Maarten de Boer and Alex Corwin[136,137]. As it can be seen in Fig. 22, it consists of a micro fabricated slider that can be brought into contact with the sample of study in order to perform friction measurements. In fact, it was designed in order to test Amonton's friction laws in the nanometric range. The Nanotractor® is capable of applying F_v up to the mN range with high accuracy and its high sliding frequency (up to 80000 cycles per second) makes it useful for wear studies. It can be also used as a high precision micro actuator and micromanipulator, although for the moment is not commercially available.

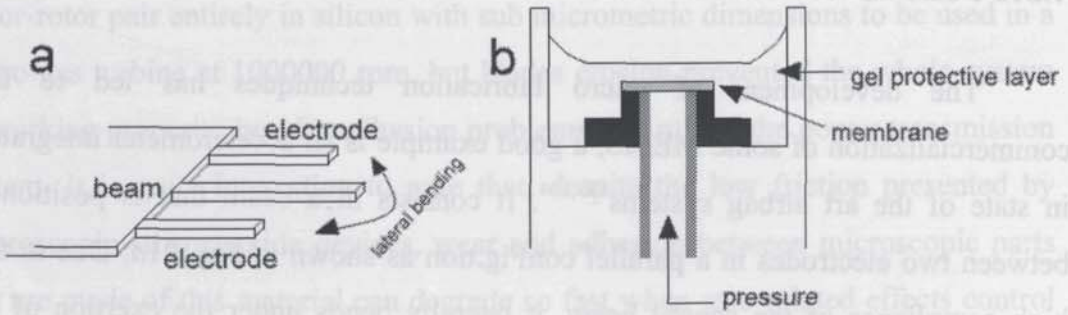

Fig. 21. Examples of commercial MEMS. a) micro-accelerometer. When acceleration changes, the central beam bends laterally, modifying the capacitance of the system. The complete device consists on an array of electrode-beam-electrode units oriented in perpendicular directions and suspended on springs so as to be sensitive to accelerations in all axes. b) Pressure sensor. As pressure changes, a change of resistivity is detected by the piezoresistors placed in the membrane.

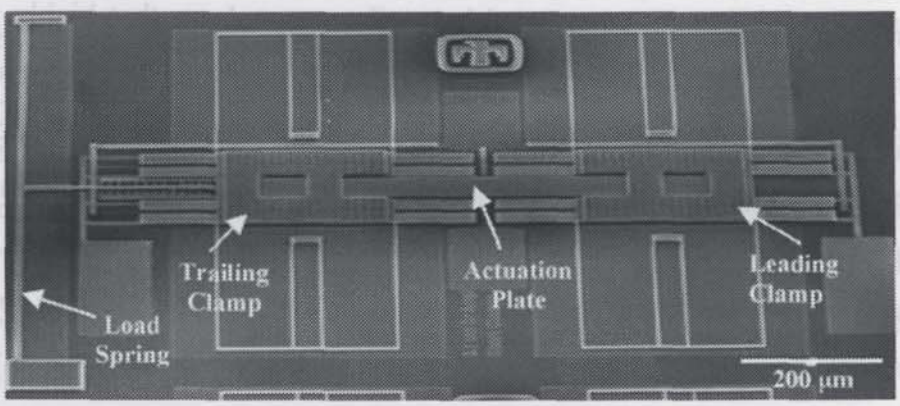

Fig. 22. Scanning electron microscope image of the Nanotractor®. The design incorporates a tangential force actuation plate in its central section, and frictional clamps on its two ends. In the clamps, load is applied electrostatically but borne mechanically to develop friction forces. To obtain motion, the leading clamp is fixed in place with a large voltage. The plate is then actuated by attracting it towards the substrate. Because the actuation plate is now bending, the trailing clamp, which is not loaded, slides a short distance (40 nm) towards the leading clamp. The trailing clamp is now held fixed with a large voltage, and the voltages on the leading clamp and plate are turned off. The leading clamp then slips forward. This cycle is repeated over and over to obtain large-scale motion with very high precision. Image extracted from www. sandia.gov/news/resources/ releases /2004/micro-nano/nanotractor.html

4.4 NEMS

An interesting NEMS example is the Millipede® concept developed by IBM Zurich[138-145] (Fig. 23). As an attempt to obtain highly density storage devices, the

Millipede® consists on a vast array of AFM-like cantilevers with sharp tips that are able to write and read a silicon surface covered with a polymeric film. The writing process is based in the local thermal fusion of the polymer by means of a tip heated up to 400ºC that creates a hole in the range of 10-50 nm (a *bit* of information). The reading process is also performed by the cantilevers array and is based in the dependence of the cantilevers thermal conductivity with the distance to the silicon substrate. Then, when a tip falls into a hole, the system is able to detect it because there is a resistance decrease. The information erasing is performed by heating the sample and melting the polymer, which redistributes uniformly on the surface replenishing the holes. The main problem of this system comes from tips wear. To understand that, we must compare it with a standard AFM, where tip wear is also noticeable after performing several images (the wear is highly dependent of the operation mode and inversely proportional to your AFM skills). Nevertheless, AFM has a feedback system that maintains a constant cantilever deflection, while the cantilevers in the Millipede® system bump wildly on the surface as the whole system scans the polymeric surface. For this reason, and although huge efforts are being devoted to solve the problem, there is still a lot to do.

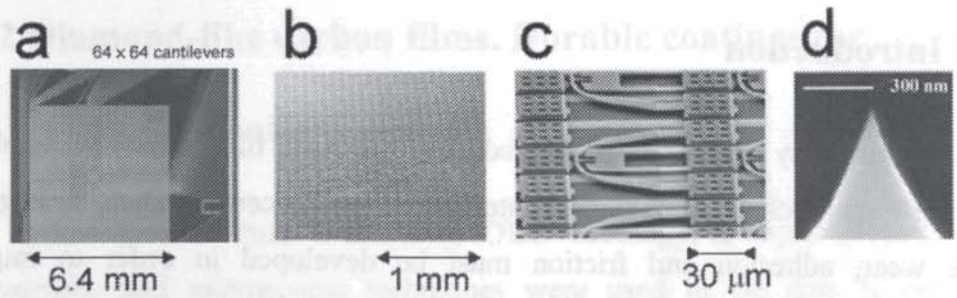

Fig. 23. Millipede® project, devoted to create a high information density write-read device. a) Whole array of 4096 AFM-like probes. b) and c) Zooms of the device, where individual cantilevers can be resolved. d) SEM image of an individual tip apex, used as a writing and reading tool. Images extracted from www. zurich.ibm.com/ st/storage/ millipede.html

4.4.1 NEMS for biological applications

NEMS have also been applied to biological issues such as electrophoretic separation[146], biochemical analysis[147] or drug delivery[148]. Nevertheless, an application that I consider as a breakthrough is the development of immunoinsulation biocapsules, developed by Desai et al.[149] These biocapsules consist of two silicon membranes bond together creating a closed environment where drugs or cells can be enclosed. The membranes are engineered to have pores as small as 6 nm, size that is large enough to let the nutrients enter the biocapsule but that blocks natural antibodies, creating a safe environment. The main problem with this and other biologically oriented NEMS is the adhesion of proteins and cells to the exterior of the device, which leads to the pore clogging and subsequent cellular death. Nevertheless, several strategies based on the functionalization of the device surface with hydrophobic molecules have proved to avoid undesired adhesion of antibodies and proteins to these bioNEMS.

4.5 COATINGS FOR MEMS AND NEMS

4.5.1 Introduction

As you may suspect by now, reducing the scale of our devices implies a whole new approach as far as surface interactions are concerned. Then, strategies to reduce wear, adhesion and friction must be developed in order to improve durability and reliability. In this direction, there are two main approaches to the problem. The first one is depositing a hard coating on our device. As this kind of coatings are somewhat out of the scope of this thesis, I will just focus in diamond-like carbon (DLC) films, which have been partially studied[150-153]. In the past, a lot of work has been done in this field, mostly focused on improving the performance of microelectronics products[154,155]. To give an example, tons of papers and patents have been devoted to improve the coating deposited on hard-disk dispositives[156-158]; as data storage capacity increases, the reading and writing devices must fly closer

to the surface and then attaining low friction coefficients is mandatory. Then, DLC and related films have become a promising option.

The second approach consists on covering the surfaces with a molecular monolayer with interesting tribological properties. The advantage of this method is that the coating can be done using soft chemistry methods, which are convenient and cheap. Besides, as molecules can be functionalized, the performance of the coating can be tailored to meet the desired surface properties. As this kind of coatings have been studied in much more detail and are a key part of the work presented here, they will be introduced more extensively. Specifically, three families of molecules will be reviewed, that is, alkanesilanes[159], alkanethiols[160,161] and fatty acids[162,163] which, although they are not lubricants in a strict sense, they provide simple models in order to understand the nature of nanotribology and nanomechanics from scratch. In this point, and despite the exciting introduction about MEMS and NEMS, I must confess that I have always been more interested in the basic concepts of nanomechanics than in the possible applications and implementation in the real world, so all the works presented in this thesis follow this train of thought.

4.5.2 Diamond-like carbon films. Durable coatings for microelectronics industry

Although literature concerning DLC tribology is considerable, mostly macroscopic and microscopic techniques were used in the past to assess the response of these layers to the exertion of a variable F_v[164]. Nanotribological measurements, mostly using LFM, are not so common although in the last years the number of references increases noticeably.

Crossley et al.[165] reported a pioneer work concerning the comparison of experimental measurements of μ for DLC films fabricated by ion-beam assisted deposition and chemical deposition. In this work is very clear that the topography of the obtained samples has to be taken into account when it comes to perform

LFM experiments, as rough samples can distort the friction loop and mask the results. The applied F_v on the samples ranged from 0 to 7000 nN, so the presented experiments fall more easily in the micro-scale range than in the nanotribological measurements. They obtained μ values ranging from 0.03 to 0.2 after applying 10000 friction cycles in the same area, which are comparable to macroscopic results obtained in similar samples[166]. An interesting concept related with the magnitude of applied F_v values was discussed; although F_v values applied in macroscopic experiments (pin-on-disk or ball-on-disk techniques) can be millions of times higher than those applied in LFM experiments, the applied pressure is comparable[167,168]. A posterior work released by Bhushan et al.[169] coped with the different frictional response of a Si(100) surface before and after being coated with DLC as studied by LFM. Interestingly, they observed that the μ value strongly depended on the tip radius and the humidity (0.02 at 0%RH and 0.12 at 50%RH) for the uncoated surfaces while it was almost independent of these factors after the DLC film was applied (between 0.02 and 0.04). They attributed this difference to the reactive nature of the Si(100), which highly interacts with water forming a liquid meniscus and, consequently, increasing friction and the μ value. Instead, the hydrophobic surface of the DLC coating does not interact favorably with water and the sliding interface is not affected by any adhesive force promoted by hydrophilic-hydrophilic interactions. They nicely reinforced these conclusions etching the DLC surface, process that activated the sample and made its nanotribological response dependent on water, as the naked Si(100) surface. Nevertheless, the μ value for etched DLC surfaces was always lower than that of Si(100) samples, highlighting the intrinsic low frictional response of the coating.

A couple works released by Santos et al. deal specifically with the response of DLC films when LFM experiments are performed, gaining further insight in the nanotribology of these films. In the first work[170], the experimental values of μ were compared for DLC and MoS_2 films, which are also considered low friction coatings[171-173]. While the mean μ value for DLC was 0.13, μ value for MoS_2 was 0.32. Besides, the distribution of values was noticeably narrower for DLC than for

MoS_2. This was attributed to contamination of the MoS_2 surface, which was experimentally demonstrated by micro-Raman experiments. While DLC surface remained practically unchanged during 45 days (as assessed by LFM experiments), the MoS_2 film oxidized forming MoO_3, which is responsible for the high μ values obtained on those samples. Having reported the suitability of DLC films as low-friction coatings in the nanometric range, Santos et al. studied the influence of the sputtering deposition parameters in the μ magnitude[174]. The most interesting result consisted on the variation of μ value as a function of the quantity of N_2 flowing in the chamber. High quantities of N_2 increased μ value up to 0.18. Although the reason was not very clear, they hypothesized that the surface composition is altered by the gas flow, which changes the proportion of C-H surface bonds and the quantity of surface oxygen.

4.5.3 Alkanethiols. Robust coatings for metals.

Alkanethiols have proved to be one of the most reliable monolayers when it comes to talk about durability and robustness[175,176]. As the thiol group bonds covalently to a variety of metals[177], the monolayer is difficult to remove when shear movements are performed between sliding surfaces, so they have become one of the best options to reduce friction in MEMS[178] and NEMS[179]. These molecules are composed by a thiol headgroup that attaches to the metal substrate and by an alkyl chains that can be functionalized so as to meet the required tribological properties[180]. Differently from the hard coatings discussed previously, alkanethiols provide true lubrication in the nanometric range in a very controlled fashion. In this chapter, we will focus on the nanotribological properties of the most common alkanethiols from the experimental and fundamental point of view, but also on its structure and behavior as a certain F_v is applied, as this is the topic we have dealt with in the results section.

4.5.3.1 Frictional properties of alkanethiols

4.5.3.1.1 Effect of temperature

I would like to begin this section talking about one of those papers that you read so many times while struggling with a nanotribology PhD thesis. And this is the work by Zhang et al.[181], who provided a really useful methodology to attain the always challenging goal of performing reproducible LFM measurements; the method consists on measuring the μ value of a reference substrate (they used mica) several times until a reproducible value is obtained. During the process, the tip R increases due to wear until a stable shape is reached, which is a mandatory requirement so as to obtain meaningful results. They confirmed that after performing a thermal treatment to an alkanethiol sample, F_f increased by a factor of 10. In fact, the treatment converted the monolayer from the $(\sqrt{3} \times \sqrt{3})R30°$ phase into the $(p \times \sqrt{3})$ stripe phase, which presents lower molecular density[182,183]. It was suggested that the presence of voids in the structure made possible the excitation of gauche defects in the hydrocarbon chains, increasing the F_f value. Similar results concerning the effect of molecular ordering on the nanotribological properties and the sensitivity of LFM measurements had also been suggested in experimental[184,185] and simulation works[186-188]. Similarly, if the alkanethiols are cooled down below the phase transition (around 100ºC, depending on the length of the alkyl chain), F_f value decreases due to the limited mobility of the molecules, which results in a monolayer with better compactness and, consequently, less opportunities to dissipate energy exciting molecular deformations[189]. It must be noted that all the LFM measurements commented until now were performed at room temperature, that is, the monolayer was annealed for a certain time but then the experiment was performed at room temperature. For this reason, a certain time was lag before performing experiments once the monolayer was cooled below the transition temperature (T_M). To the best of my knowledge, just Fujita et al.[190] have performed in-situ LFM experiments with variable temperature, which gives an idea of the experimental difficulties that must be overcome so, despite being a pretty basic

work, it deserves to be mentioned as a technical breakthrough. They demonstrated that a dodecanethiol monolayer on gold presents a linear relationship between F_v and F_f but also a friction peak around 240K, fact that had been predicted by simulation studies and attributed to the rotational transition point of the monolayer, which is around 240K[191,192].

4.5.3.1.2 Chain length and chain functionalization

Li et al. studied the different frictional behavior of thiols with alkane chains of 8 to 18 carbon atoms, concluding that μ value decreases noticeably as the chain length increases (from 0.13 for C8 thiols to 0.023 for C18 thiols)[193] although they did not propose any physical reason for the phenomenon. The measured μ value for the bare gold substrate was 0.28, which points out the outstanding friction reduction achieved by the alkanethiol monolayer deposition. The dependence between F_v and F_f was found to be linear at high F_v values but noticeably non-linear in the low loads regime, as expected from the Hertzian contact model, which predicts a $F_v^{2/3}$ law for a spherical tip[106,115]. In order to maintain the integrity of the monolayer and to test the frictional properties of its outermost part, F_v values not bigger than 60 nN were applied while maintaining 30% humidity level. The functionalization of the tip with alkanethiols showed that, unfortunately, reality can be much more complex than was expected; when using a tip coated with a carboxylic acid terminated alkanethiol, friction was higher on carboxylic acid and hydroxy- terminated alkanethiol SAMs on gold than on methyl- terminated monolayers[194]. As expected, the higher friction and μ values were recorded for similar sliding interfaces, suggesting that the strong F_f for acid-acid interfaces is due to the creation of hydrogen bonds[195-197]. The striking fact was that, although the F_f value was dependent of the chain length for methyl terminated layers, the dependence did not exist for acid carboxylic and hidroxy- terminated monolayers. It was suggested that, while the length of the chain for non-functionalized alkanethiols plays a key role in the stability of the layer (the longer the chain, the more compact and difficult to deform), the strong electrostatic and hydrogen bond interactions arisen between the polar groups in functionalized molecules can mask the stabilization

due to van der Waals interchain interactions. Then, even short chain thiols functionalized with carboxylic and/or hidroxy- groups can form well ordered and compact layers.

It was clear that the chain length and its functionalization were key factors to understand the nanotribology of alkanethiol monolayers. Nevertheless, some structural factors were still to be discovered. In this direction, Zhang et al., by means of molecular dynamics simulations, proposed that thiols should show friction anisotropy depending on the scanning direction. In other words, F_f should be minimum when the tip scans in the direction of the molecular tilting and maximum when it scans against the tilting[198], as it had been previously observed in glycerol layers by means of LFM experiments[199].

I also would like to mention the works released by Brewer et al.[200,201], which nicely sums up the chain length effect, the dependence of friction with functionalization and also investigates other parameters as sliding velocity, monolayer ageing and effect of the substrate (gold and silver) on the molecular packing density and its consequent nanotribological response.

A topic that deserves a special attention is the nanotribology of fluorinated alkanethiols. As we all know, Teflon is a very common low-friction coating used in a thousand applications. Nevertheless, Kim et al. found that terminal-fluorinated alkanethiol monolayers on gold show a noticeably higher friction than their non-functionalized counterparts[202]. They argued that the friction increment was due to the different chemical composition of the outer part of the chains but also to the different size of the methyl and the F- groups. Then, as the F- heads are bulkier than the methyl heads, a certain structural tension was induced in the whole layer, providing ways to dissipate frictional energy in the form of molecular deformation due to structural defects and mismatch between the zigzag alkyl chains. Further experiments demonstrated that the strong polar nature of the F- groups could interact with the AFM tip, which is polar and sports a certain net charge[203], increasing the adhesion between the sliding interfaces[204].

4.5.3.1.3 Humidity effect

As friction is an interfacial process, humidity has a huge effect on frictional properties as it is present on all surfaces in normal conditions. Nevertheless, depending on the hydrophobicity or hydrophilicity of the sliding surfaces, the effect changes dramatically. To exemplify that, a comprehensive and extremely clear paper released by Li et al.[205] dealt with this issue in a very elegant way; they prepared mixed monolayers of two thiols, one of them methyl terminated and the other, hidroxy- terminated and measured their μ values for different proportions of thiols as a function of humidity. They reported that, while the fully hydrophobic thiols, that is, the $-CH_3$ terminated, show a low μ value (ca. 0.05) no matter the humidity, the monolayers with hydrophilic thiols have tribological properties that are extremely dependent on the water presence, reaching μ values as high as 0.5 for pure –OH terminated thiols at 10%RH. Similar experimental[206] and simulation[207] results had been previously reported for alkanes on Si(111) and for bare mica, which is a strongly hydrophilic surface and, therefore, highly dependent on humidity as far as surface phenomena are concerned. To understand this effect, we may think that water forms layers on hydrophilic surfaces and that this "coating" increases F_f value[208,209]. Apparently contradictory results were observed for alkylsilanes deposited on mica, where a dependence of the μ value with humidity was reported despite of the hydrophobicity of the layer. In that case, the authors argued that the lack of compactness on the monolayer exposed parts of the substrate (mica), which was responsible for the μ value variation.

Similar results were reported by Qian et al.[178], who also reported that bare gold, the most common substrate for thiols), show a F_f value peak around 40%RH and that for higher humidity levels F_f magnitude decreases to reach the same value as in the absence of water. These data seem to be in contradiction with the results obtained for hydrophilic thiols but the authors point out that, while water ends up forming layered structures, at moderate humidity level the water molecules are highly adhered to the hydrophilic gold substrate and that viscous and confinement effects stand for the friction increase[178]. They went a step further and modified the

AFM tips with hydrophobic alkanethiols; when a monolayer of hydrophilic thiols was scanned, the μ value was nearly independent of humidity, in concordance with all previous data.

4.5.3.2 Alkanethiols under vertical compression

The orientation and packing structure of alkanethiols has been widely studied and several different phases have been detected depending on the layer compactness and the experimental conditions of pressure and temperature. For the interested reader, I would suggest the work of G.E. Poirier[210], who followed the growth of these monolayers on Au(111) under UHV conditions by means of STM[211]. In ambient conditions, alkanethiols form a commensurate $(\sqrt{3} \times \sqrt{3})R30^{\circ}$ lattice, with the alkyl chains tilted ~30°[212] respect to the surface perpendicular. The nature of this tilting has been a matter of extensive research along the years but was Ulman[213] who, adapting a work released by Outka et al.[214] concerning calcium arachidate Langmuir-Blodgett monolayers, proposed the most accepted explanation; the alkanethiol molecules tilt in order to maximize the van der Waals interactions between their hydrocarbon chains, providing an optimum zigzag backbone interlocking (Fig. 24*a*). Nevertheless, there was no experimental evidence to support this model, as Ulman studies were purely computational[213]. The first serious experimental attempt was pursued by Tupper et al.[215], who reported some Interfacial Force Microscopy (IFM) experiments where the compression of alkanethiol monolayers was investigated with nanometric resolution. They found no trace of tilting discretization, as the monolayer deformed in a continuous way, which was in contradiction with the interlocking model. Nevertheless, further AFM topographic work concerning alkylsilane monolayers demonstrated how small islands decrease their height in discrete steps while F_v value[216] is increased. According to this and leaning on the Outka model[214], it was proposed that several tilting angles (θ) that permitted favorable van der Waals interactions between chains were possible. These suggestion was refined in a comment to *Physical review Letters* in order to include still more possible angles[217], attending to the

possibility of molecular rotation. Despite the good results, the model did not explain all the heights that were observed while compressing alkanethiol islands deposited on gold and it was the development of an extended model which expanded the chain interlocking concept to 2 dimensions[218], that is, molecular tiltings in two directions (θ_x and θ_y) in order to explain all the possible favorable interactions in the hexagonal alkanethiol structure, the one which proved to explain all experimental results (Fig. 24*b*). The necessary F_v value to trigger the tiltings was 3.3 nN which, after applying Hertz model and considering the experimental tip R, corresponded to a 0.5GPa pressure[218]. The authors proposed some interesting conditions that were necessary for the interlocking model to work; first of all, it is necessary a certain amount of defects in the monolayer in order to accommodate the extra molecular area that results from the θ increase and secondly, the necessary F_v value to trigger the tilting process highly depends on the number of vacancies and the size of the alkanethiol islands. Then, the higher the number of defects and the smaller the island size, the lower the needed F_v value to trigger the molecular tilting[219].

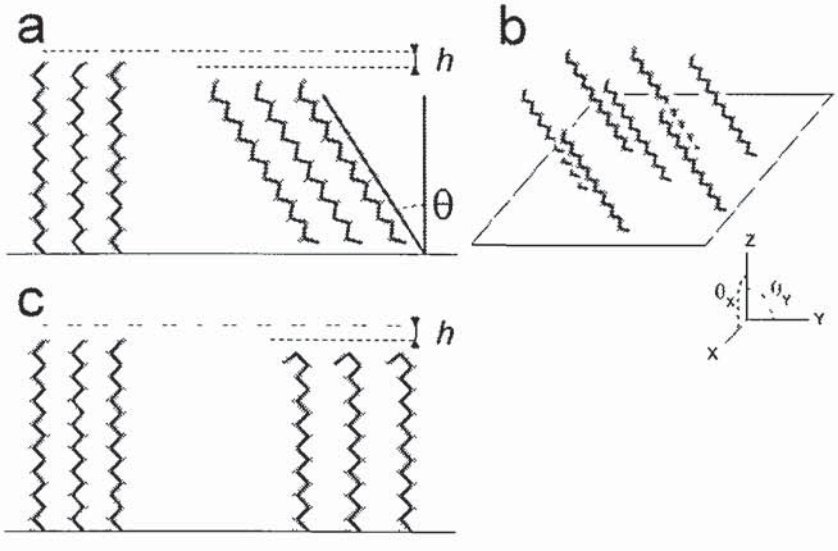

Fig. 24. Different mechanisms for alkanethiol deformation under compression. a) 1 dimension model proposed by Outka[214], Ulman[213] and Barrena[220], where the thiols tilt a certain θ angle so as to maximize van der Waals interactions and, consequently, alkyl chains interlocking. a) Extended model in 2 dimensions where two angles (θ_X and θ_Y) are considered. c) Deformation by terminal gauche defects creation. h stand for the monolayer thickness diminution as an external pressure is applied.

Another proposed explanation for the deformation of monolayers under pressure is the creation of gauche defects (Fig. 24*c*). A pioneer work by Hartig et al.[221] calculated that the energy necessary to create gauche defects in the terminal carbons of alkyl chains is in the range 15-25 kJ/mol, which is the range of energies that an AFM tip can apply to the samples. Interestingly, the height reduction observed during compression experiments (h) is compatible with this model but also with the tilting angle theory, so it remained unclear which explanation was closer to the real phenomenon. MonteCarlo simulations concluded that alkanethiol monolayers could be subjected to 25% of height reduction before deforming plastically[191,222], but that an initial molecular tilting underwent just after the application of a minimum F_v. It was also concluded that the pressure reduced the number of defects in the inner part of the layer but that increased the number of terminal gauche defects[222]. Vibrational spectroscopy experimental results corroborated the simulations and it was proposed that the most defective monolayers were more prone to undergo irreversible deformation under compression[223]. Besides, a high degree of disorder in the terminal ends of the chains was detected and related with the presence of gauche defects. More recent Ultrafast Dynamics of Shock Compressions experiments revealed different behaviors as a function of the chain lengths[224]; chains with an odd number of carbon atoms forces the methyl groups to tilt elastically under the exertion of an external pressure while chains with an even number of carbons deform viscoelastically forming gauche defects. Although is less likely than the formation of terminal gauche defects, these deformation processes are also possible in the chain core. As you can see, there is still a lot of work to do so as to clarify which is the alkanethiol monolayers deformation mechanism.

Although alkanethiols deformation under pressure can seem a secondary issue, it is a really important one because the results obtained on these kinds of layers can be extended to all monolayers sporting alkyl chains, which are the vast majority. Besides, these studies provide invaluable information about the interactions between individual molecules down to the PicoNewton level.

4.5.4 Fatty acids. Simple molecular models

Fatty acids are a family of molecules composed of a carboxylic acid headgroup and an alkyl chain[225,226] and that play an important role in biological systems[227,228]. Fatty acids are very useful molecular models because of their simplicity and, although the carboxylic groups do not bind covalently to the substrate as in alkanethiols case, they have proved to be suitable low-friction and high-durability coatings. For example, stearic acid (SA) monolayers noticeably reduce the friction response of polyethyleneimine coated silicon substrates[229] and lignoceric acid (LA) was used as a support for C60 particles, which are considered as extremely powerful lubricants both by its surface properties and geometrical shape[230].

Because of their linearity and long alkyl chain, fatty acids usually pack in an ordered way[231-233], forming compact and reproducible monolayers. This structural compactness is also promoted by the carboxylic acid groups; having a similar radius as the hydrocarbon chains, they do not interfere in the optimization of van der Waals forces between chains[213,214,216] as could be the case for hydroxysilane groups in alkanesilane monolayers[185,234]. Besides, monolayers with a controlled molecular area can be prepared using the Langmuir-Blodgett (LB) transfer technique (Fig. 25), so Force Spectroscopy and LFM experiments performed on this kind of samples can shed light on the magnitude of the different interactions that modify monolayer cohesion. In this direction, interchain van der Waals interactions can be quantified, as well as the electrostatic forces and hydrogen bonds that exist between the polar heads, which can be modified by adding ions in the subphase prior to the extraction on a solid support. For all this, we chose to prepare arachidic acid (AA) LB monolayers so as to understand and explore the nature of all these different interactions and how they affect the nanomechanics of similar systems as alkanethiols, alkanesilanes or phospholipid structures. For the sake of simplicity, I will talk about AA monolayers most of the time, although the exposed concepts can be extended to the vast majority of the fatty acids, once the differences arisen due to chain length or unsaturations are taken into account.